

# Aerodynamic reduced-order Volterra model of an ornithopter under high-amplitude flapping<sup>☆</sup>



C. Ruiz, J.Á. Acosta\*, A. Ollero

GRVC Robotics Laboratory, Universidad de Sevilla, 41092 Sevilla, Spain

## ARTICLE INFO

### Article history:

Received 3 February 2021  
Received in revised form 6 December 2021  
Accepted 4 January 2022  
Available online 12 January 2022  
Communicated by Huihe Qiu

### Keywords:

Ornithopter aerodynamics  
Large flapping amplitude  
Bio-inspired UAV  
Volterra model

## ABSTRACT

The unsteady aerodynamics of flapping low-aspect-ratio ellipsoidal-wings in ornithopters is analyzed and modeled by the use of three dimensional Computational Fluid Dynamics (CFD) simulations. The range of interest is high amplitude, moderate frequency flapping, and low to moderate angles of attack at Reynolds around  $10^5$ , where autonomous ornithopters like GRIFFIN are able to perform complex maneuvers such as perching. The results obtained show that the Leading Edge Vortex is produced above a certain Strouhal and angle of attack at downstroke. The frequency response of the aerodynamic loads are compared with the classical analytical models, observing that analytical models based on absence of viscosity and small perturbations are not appropriate for the range of interest. Through the 3D CFD aerodynamic loads database, a finite memory Volterra model is identified in order to predict the characteristics of forces and moments produced by the flapping wing. A good agreement with the 3D CFD simulations has been found by considering a reduced-order model depending on the effective angle of attack of the surrogate airfoil located at 70% of the semi-span at three-quarters chord on the airfoil, in agreement with the literature. Finally, a methodology for validation with a high-accuracy Motion Capture System and without the need of wind tunnel is proposed. As a result the proposed model provides better estimates than classical analytical ones.

© 2022 The Author(s). Published by Elsevier Masson SAS. This is an open access article under the CC BY license (<http://creativecommons.org/licenses/by/4.0/>).

## 1. Introduction

The efficiency and maneuverability, both in gliding and flapping [1], of bird flight has fascinated scientists throughout history, a fact that can be shown in the diversity of ornithopter prototypes developed, such as the Festo Smart Bird [2], Robird [3], Robo Raven [4] and E-FLAP [5]. Currently, the emphasis in ornithopter research is mainly focused on the aerodynamics of flapping wings and design as e.g. in [6–11], but at micro/small scale and in experimental setups, unlike here that we focus on high-amplitude flapping in large ornithopters with validation in flight using a high-precision motion capture system.

The optimization of the aerodynamic loads such as lift can enhance the payload of the ornithopters such as the GRIFFIN's prototype E-FLAP [5] (see Fig. 1), being able to improve the sensing and computational capabilities, thus allowing fully autonomous flight and perching. Moreover, aerodynamic models are also strongly

needed to optimize model-based control and planning algorithms. However, while simple analytical models subject to various hypotheses are practical in the preliminary stages of ornithopter design, they become overly complex when trying to model flow more accurately, as it is the case of high-amplitude flapping. Thus, Computational Fluid Dynamics (CFD)-based models provide a useful tool in the middle stages of ornithopter development. Post-processing techniques provide a broad view of the phenomena that occur in the fluid in the Unmanned Aerial Vehicle (UAV) operating range, facilitating the type of the model to identify. Putting it all together makes aerodynamic modeling of high-amplitude flapping wing a challenging task in terms of accuracy and complexity, since involves unsteady viscous phenomena on three dimensional flow.

**Classical analytical models and corrections.** Unsteady aerodynamic models reflect the dependence of aerodynamic forces with the airfoil states, beyond quasi-steady models that assume that the forces produced depend only on the position of the wing with respect to the airflow but memoryless. Researchers have demonstrated that this aerodynamics do not capture the real phenomenon of flapping wing at intermediate-range Reynolds [12], [13]. Early models developed for unsteady aerodynamics were those of Wagner [14] and Theodorsen [15], for the lift and mo-

\* The authors acknowledge support from the European Project GRIFFIN ERC Advanced Grant 2017, Action 788247.

\* Corresponding author.

E-mail addresses: [craez@us.es](mailto:craez@us.es) (C. Ruiz), [jaar@us.es](mailto:jaar@us.es) (J.Á. Acosta), [\(A. Ollero\)](mailto:aollero@us.es).

## Nomenclature

$\alpha$	Static angle of attack.	$V$	Free stream velocity .....	m/s
$\alpha_s$	Wing-body fixed angle.	$x, y$	Position in inertial reference frame [m], input-output variables of a generic system.	
$\alpha_{eff}$	Effective or induced angle of attack.	$y_{ref}$	Reference position in span of surrogate airfoil.....	m
$\bar{s}$	Non-dimensional Laplace variable.	$\bar{c}$	Wing mean chord .....	m
$C$	Theodorsen's function.	$\lambda$	Ridge Regression regularization coefficient.	
$\mathcal{H}$	Volterra Linear kernel.	$\mu$	Air viscosity.....	N s/m <sup>2</sup>
$\Phi$	Wagner's function.	$\rho$	Air density .....	Kg/m <sup>3</sup>
$\Psi$	Volterra functional.	$\theta$	Wing position in flapping, pitch angle.	
$\sigma$	Discrete memory index.	$k$	Reduced frequency.	
$\tau$	Discrete time index.	$Re$	Reynolds number.	
$\Theta$	Random variable.	$S$	Wing surface .....	m <sup>2</sup>
$A, B$	Generic matrices of a linear system.	$t$	Dimensional time.....	s
$b$	Wing semi span, half chord .....			
$c$	Wing's root chord .....			
$f$	Flapping frequency.....			
$h$	Airfoil heaving amplitude .....			
$I_{yy}$	Pitch moment of inertia.....			
$L, D, M$	Lift, Drag and pitch Moment in aerodynamic reference frame.			
$M$	System memory in time steps.			
$m$	Ornithopter mass .....			
$N$	Time series length.			
$St$	Strouhal number.			
$u, v, w$	Linear velocities of ornithopter in body frame.			

Acronyms

CFD	Computational Fluid Dynamics.
LEV	Leading Edge Vortex.
MCS	Motion Capture System.
NMSE	Normalized Mean Square Error.
RANS	Reynolds-Averaged Navier Stokes equations.
ROM	Reduced Order Model.
UAV	Unmanned Aerial Vehicle.
UDF	User-Defined Function.
WTW	Wing-Tip Vortex.



Fig. 1. GRIFFIN e-flap prototype.

ment forces in airfoils, derived from the well known linearized potential theory and therefore assuming their hypotheses. The first represents the lift evolution after a change in the effective angle of attack at 3/4 chord by the impulse response and the convolution integral. On the other hand, Theodorsen proposed a frequency response model for the same problem, and highlighted the relevance of the reduced frequency in performance. However, both models were shown to be equivalent later on [16]. A year later, Garrick [17] made use of the linearized potential theory and the Theodorsen function to derive a compact model of the propulsive forces caused by an airfoil performing small oscillatory heaving and pitching. This theory has been enhanced recently by Feria [18], with the use of the Vortical Impulse Theory. Assuming that a flapping wing's airfoil in heaving could be interpreted as an infinite wing in such movement, surrogate models found similarities between the performance of the airfoils at given points along the span and that of the three-dimensional flapping wing. Based on Wagner's Indicial Response, Jones [19] proposed a correction of the Theodorsen's Theory with the aspect ratio for three-dimensional wings. Subsequently, some corrected models based on the Lifting Line Theory were derived from the Wager's step response in or-

der to model arbitrary displacements of the wing, as e.g. Delaurier [20].

**Low Reynolds and high amplitude modeling.** At present, various investigations have been carried out on the aerodynamics of flapping wings and aeroelasticity which is being studied as a potentially performance-enhancing phenomenon of flapping wing systems at low Reynolds. Moreover, there is a marked tendency in flap wing research to study insect and bird flights separately. While insects generally operate at very low speeds through high beat frequencies and complex wing kinematics, where viscous phenomena mainly occur [21], [22], [23], birds fly at higher speeds, where circulatory effects are not negligible [24]. A review of models for insects proposed till the date can be found at [25] of both integral and circulation approach. The authors conclude that the Ansari model, a quasy-3D model derived from potential flow equations was the most satisfactory model to date. However, it was only validated for a Reynolds of the order of  $10^2$ , typical in insects. On the other hand the authors derived a numerical model for insects hovering [26].

Although classical models based on the lifting line and potential theory are still widely used [27], due to the development of CFD and experimental techniques, the underlying phenomena at intermediate-range Reynolds has been thoroughly studied, both in airfoils and three dimensional wings. Thus, several researchers agree that the Leading Edge Vortex (LEV) is the cause of hyper-lift effects in flapping wings at moderate Strouhal numbers in the Reynolds range of  $10^4 - 10^5$ , that includes insects and vertebrates [28], [29], [12], [30]. Reference [31] presents a recent review on the state of the art of the aerodynamics of flapping airfoils, and concludes that further study of the performance of 3D flapping wing aerodynamics is necessary to better understand the flight of birds in order to achieve efficient real applications.

Due to the increase of complexity, in recent years Reduced Order Models (ROM) have been identified for the operating range of interest, base on numerical and experimental data. A complete revision of unsteady aerodynamics data-driven modeling methods

can be found at [32]. The strengths and weaknesses of each approach that has been developed are analyzed, emphasizing those based on identification. Modeling unsteady aerodynamics is classified in three methods: Theoretical, computational and data-driven methods. Brunton et al. [33] proposed a semi-empirical state-space representation of Theodorsen's lift model, by identifying the circulatory and added mass parameters empirically at intermediate-range Reynolds flows. Zakaria et al. [34], [35] identified, by means of a wind tunnel experiments, the empirical frequency response of a plunging wing at high angles of attack, resulting in a lift enhancement compared to Theodorsen's prediction at certain frequency. Boutet et al. [36] extended the Wagner theory to three dimensional wings by using the lifting line theory, maintaining the small perturbations hypothesis. Taha et al. [37] included the effects of the stall modeled by the lift-alpha slope in the Wagner's Indicial Response, using the Duhamel's principle and obtained a ROM for insects at high reduced frequencies. Currently [38] compare Navier Stokes simulations of a airfoil and the Theodorsen transfer function revealed that the differentiation between circulatory and non-circulatory lift is diffuse under certain conditions, concluding that it must contain a "viscous circulation" term.

Finally, regarding with Volterra approaches, Silva et al. [39], [40] proposed the Volterra theory to high velocity unsteady aerodynamic responses analysis; Cummings et al. [41], [42] applied the Volterra theory to X-31 airplane in order to identify transonic responses and pitching characteristics; Balajewicz et al. [43] applied Multi-Input Volterra theory to transonic unsteady CFD simulations of an airfoil subject to heaving and pitching displacements; and the most related work is K. Liu et al. [44] that applied Volterra Kernel identification to flapping 3D CFD simulations, but, however, only a sole maneuver for a small angle was identified and no information about the kernel is provided. Therefore, the application of the Volterra theory for flapping wings in the literature is very limited.

In summary, this research contributes to the field of ROM for large-scale high-amplitude flapping wing ornithopters. No analytical models that predict the effect of intermediate-range Reynolds and high induced angles of attack in ornithopters operating by large beating at low velocities [35] are available. Thus, it is necessary to analyze the vortex structures that are generated, in order to better understand the lift-propulsion generation mechanisms of large flapping ornithopters in that regime. More precisely, for large ornithopters, the contributions are enumerated in detail below:

- C1. The available aerodynamic 3D-Unsteady CFD-database, in the range of Reynolds around  $10^5$  and Strouhal 0.1-1, of a semi-wing at high-amplitude flapping, at angles of attack up to 30 degrees, for which references are scarce. The methodology to obtain this database automatically and efficiently thanks to forcing an accurate initialization, shown in block diagram on Fig. 4, and the Overset Mesh approach. The CFD scheme has been verified through an available dataset in the literature.
- C2. The reduced-order Volterra model is proposed as a high perturbations generalization of the classical linear models but without separating the added mass and circulatory effects, and its applicability is analyzed. The ROM incorporates other effects that can occur at high-amplitude flapping and intermediate Reynolds.
- C3. The identification procedure of an unsteady aerodynamic ROM based on Volterra Theory with a CFD numerical database as a training set. The model is based on the hypothesis that the single input is the time history of an effective angle of attack at a proper wing's location, lift coefficient depends in a linear way on the previous states at first instance, and the memory is finite. Those assumptions have been verified by 2D and 3D aerodynamic simulations comparison to calculate the input

location, and by the model ability to accurate reproduce the training set.

- C4. The experimental validation methodology of the ROM using a high-precision Motion Capture System that provides experimental flight data, shown in the block diagram on Fig. 22. A good reproducibility has been found when raw flight data is used as input in the proposed model. This is shown as an alternative when available wind tunnel does not satisfy the requirements.
- C5. In addition, a thorough analysis of the deficiencies found in the classical aerodynamics models, that do not satisfy their hypothesis at these conditions, are also provided.

The paper is structured as follows. Section 2 is devoted to the CFD simulations for the aerodynamic database construction, which includes initial validation with available data in the literature, analysis of the unsteady 3D CFD aerodynamics and of steady simulations, in order to select the location of the surrogate airfoil. Finally, the underlying phenomena in the fluid is highlighted by vortex and pressure visualization. Section 3 is devoted to the Volterra ROM selection and identification procedure, which includes verification of the identified kernel and analysis of discrepancies with classical Wagner's theoretical model. Section 4 includes the validation methodology using a high-precision Motion Capture System and the experimental validation for lift force. Next, a discussion section where the limitations and performance of the proposed approach and results are discussed. The paper is wrapped up with a conclusion and future work section.

## 2. Computational fluid dynamics simulations

In order to gain insight into the phenomena of flapping flight, some authors proposed the resolution of Navier-Stokes equations. In reference [31] can be found most relevant CFD analysis of flapping airfoils, most of them focused on vortex visualization and correlation of two dimensional airfoils at low reduced frequency performing pitch and heave oscillations at different hinge points. However, the most challenging task on CFD simulation of 3D high rotation bodies is the efficient generation of an accurate mesh. The "remeshing" techniques were use to model the fluid volume elements along time, Bos et al. [45] among others proposed a mesh deformation technique based on radial basis functions to simulate the flow around an insect wing at Reynolds  $\mathcal{O}(100)$  using a laminar model. Nowadays become relevant the use of local mesh adaptation or Overset techniques that joined to turbulence models provides an accurate tool to solve complex flows around flapping wings [46]. Unsteady 3D numerical simulations have been performed in a commercial software for the GRIFFIN prototype wing.

### 2.1. CFD simulations setup

It is widely known that the effects of chord based Strouhal and Reynolds aerodynamic numbers govern the fluid around flapping wings in forward flight, in addition to the geometric angle of attack. On the other hand, high amplitudes of the flapping also influences the aerodynamics, not considered in small perturbation's models such as Theodorsen's model. At this study, the amplitude remains constant at a considerable magnitude and, so we will refer to the Strouhal as the chord-based Strouhal defined as follows

$$Re = \frac{\rho V \bar{c}}{\mu}, \quad St = \frac{f \bar{c}}{V}, \quad k = \pi St.$$

The wing is modeled as a rigid and thin ellipsoidal plate, which dimensions can be found at Table 1. The sections are aligned at  $\frac{c}{4}$ , where is located the stroke plane which is perpendicular to the longitudinal axis of the ornithopter.

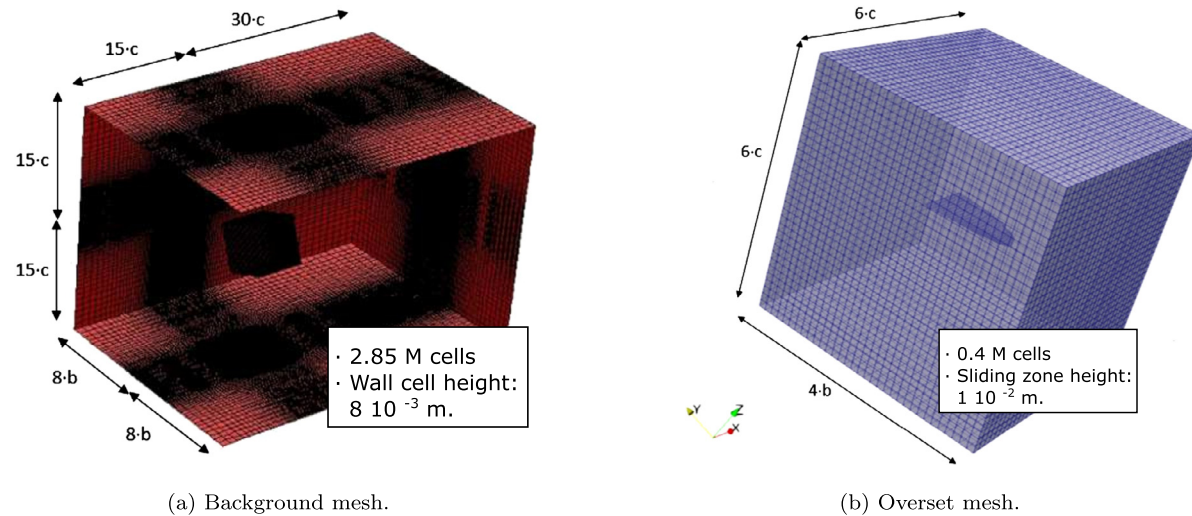


**Fig. 2.** Overset and Background mesh for unsteady CFD simulations. Boundary conditions at Background mesh are: “Inlet Velocity” at inlet surface and “Pressure Outlet” at remaining outer surfaces. “Overset interface” at Overset mesh outer surfaces and “Wall” in wing surface.

**Table 1**  
Wing model.

Wing dimensions	
Mean chord, $\bar{c}$	0.28 [m]
Root chord, $c$	0.36 [m]
Semi span, $b$	0.6 [m]
Thickness, $t$	$210^{-3}$ [m]

**Table 2**  
Parameters range of interest in the study.

Dimensional parameters	Range
Inlet velocity, $V$	(0–6) [m/s]
Flapping frequency, $f$	(0–6) [Hz]
Angle of Attack (geometric), $\alpha$	(−8 – 30) [deg.]
Non dimensional parameters	
Reynolds, $Re$	(0.4 – 1.2) · $10^5$ [-]
Strouhal (chord based), $St$	(0.1 – 0.85) [-]

The Overset Method has been used to simulate the displacement of the wing over the flapping with two unstructured meshes superimposed. The background mesh, provides the layout where slides the Overset mesh that contains the mesh of the wing surfaces. Thus, the meshes maintain their shape during simulation, avoiding the loss of quality produced by elements distortion that occurs in the dynamic mesh simulation. Fig. 2a represents the dimension of the fluid domain for each of the meshes, which have been seen to be sufficient to cover the perturbations of the wing, taking into account the reduction of the distance to the walls with the movement of the wing. The wing is centered on the Overset mesh, which is in the position shown in the Fig. 2b at the initial instant. Note that the background mesh has been refined in the moving zone so that the displacement in a time step is less than the size of the cell for the critical case, that is, maximum frequency and speed. We underscore that mesh refinements has been explored without noticeable changes.

The simulation parameters are the fluid inlet velocity, the geometric angle of attack and the flapping frequency as Fig. 3 presents. The mean angle of flapping or dihedral and the amplitude of the flapping of the wing has been fixed to 21.5 deg and 26.5 deg, respectively. The first responds to stability needs, and others are chosen responding to bio-inspired design criteria. Simulations have been performed over the entire operating range of the ornithopter, which are shown in Table 2.

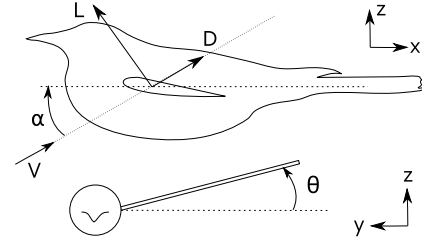


**Fig. 3.** Ornithopter's wing Degrees of Freedom.

Other simulations setups are, the Reynolds-Average Navier-Stokes (RANS) model chosen, in particular the  $k - \omega$  with Shear Stress transport, a incompressible two equation Eddy-viscosity model commonly used in intermediate-range Reynolds aerodynamics, and a pressure-velocity coupled scheme, with a first order implicit time discretization for the transient simulation. For the sake of completeness, a case for the laminar model has also been simulated, obtaining negligible differences and doubling the computing time.

Once the operating range ( $\alpha^k, V^k, f^k$ ) and CFD model is selected the simulations are automated with the methodology shown in Fig. 4, where a Matlab® interface has been also used. For each simulation the time step is selected automatically in order to obtain  $n$  points per flap, and  $N$  total flapping, hence  $f_1 = \frac{1}{n f^k}$ , where  $f^k$  is the flapping frequency at the  $k$  simulation,  $n = 100$  is the number of points per flap. The time vector will be  $j = 1 : N$ , where  $N = 3n$ . First, a steady state is simulated at each condition in order to initialize the flow before the unsteady simulation starts. A good convergence of the temporal results after 3 flapping has been observed. This convergence has been improved by previous steady simulation of the fluid field. The fluid variables solution at each element is saved in  $\mathbf{R}^k$ . The steady simulation is iterated until the error  $\epsilon$  became smaller than  $\epsilon_s = 1 \cdot 10^{-6}$ , obtaining a good convergence in the forces and moments at each time step.

Then, the steady simulation is used as initial values to unsteady simulation. The kinematics of the wing is controlled by User Defined Functions (UDF), where a chirp or sine function, namely  $f_2$ , of the position of the wing  $\Theta_j^k$  is enforced and the mesh is refreshed in each time step by this kinematics. The unsteady simulation iterates in each time step until error  $\epsilon^k$  is smaller than  $\epsilon_u$ . The total forces and moments are saved at each time step in inertial reference frame  $\mathbf{F}_j^{k,\mathcal{I}}$  and it is offline post processed in order to

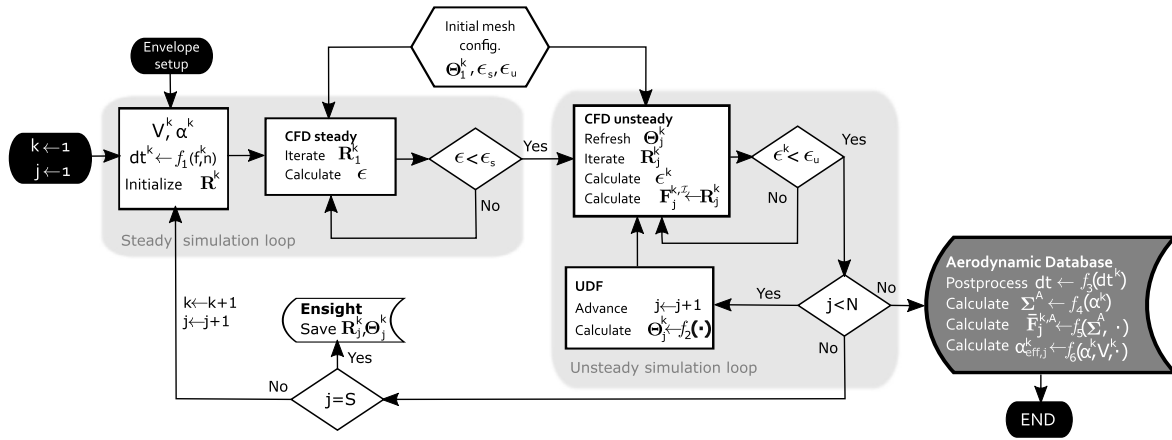


**Fig. 4.** Aerodynamic database construction process.  $k$  is the simulation identifier (a combination of incident velocity, angle of attack, and flapping frequency),  $j$  is the time step identifier for each simulation.

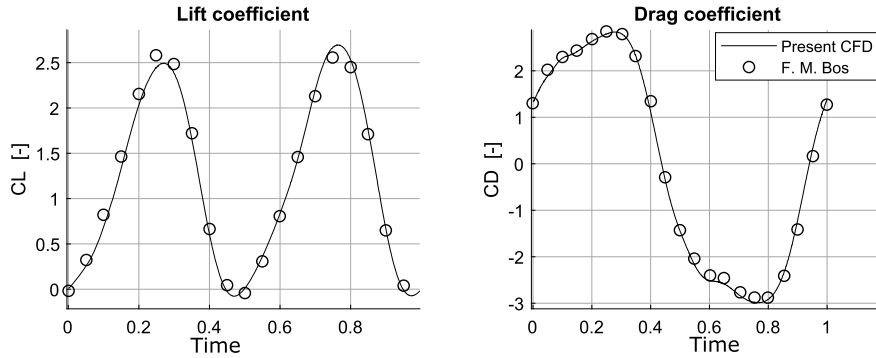


**Fig. 5.** Verification case at flapping amplitude of 63 deg, and 45 deg of pitching. The Reynolds number is 100. Black circles markers represents lift and drag coefficient from [45], black lines are coefficients from our CFD simulations reproducing the same conditions. The forces are in wing fixed reference frame.

maintain a constant time step and disposed in aerodynamic reference frame ( $f_3 = \text{gcd}(dt^k)$ ), where gcd is the greatest common divisor. Also the effective angle of attack is calculated to complete de aerodynamic database. Equations  $f_4, f_5, f_6$  are showed in detail in the next section. To finalize, the overall fluid variables  $R_j^k$  at each element are only saved at selected relevant points over the flap for vortex visualization in ensight-case-gold format due to the high computational cost.

The verification of the CFD scheme has been performed with one found in the literature for a low-Reynolds high-amplitude critical case. The model used is an ellipsoid, which performs complex figure-eight movements. The results obtained by the proposed Overset Method are shown in Fig. 5 and provides a good agreement with those offered by F.M. Bos in [45].

## 2.2. CFD results: flow visualization and surrogate airfoil

Approximately 70 simulations of flapping at constant frequency and 10 simulations varying the frequency in a linear chirp have been carried out in the previously defined range. The aerodynamic coefficients Lift, Thrust and Pitch moment defined as  $C_L = \frac{L}{\frac{1}{2} \rho V^2 S}$ ,

$C_T = \frac{T}{\frac{1}{2} \rho V^2 S}$  and  $C_M = \frac{M}{\frac{1}{2} \rho V^2 S c}$ , respectively, are shown in Fig. 8, 9 and 10 in function of the effective angle of attack ( $\alpha_{eff}$ ) which we will define next.

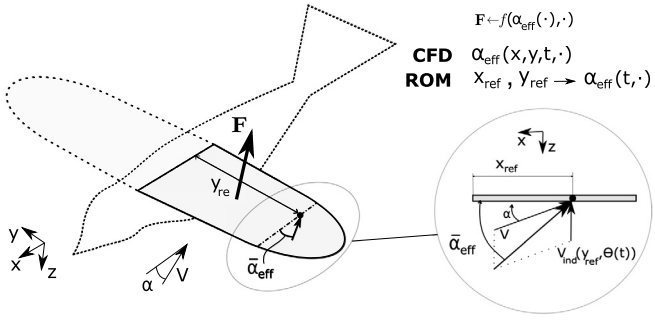
The effective or induced angle of attack of an airfoil in the wing depends on the kinematics of the wing, that is the flapping angle  $\theta(t)$ , since it is the induced angle of attack in the wing due to its movement relative to the air (see Fig. 6). It also depends on the point of the wing that we choose to be measured. It is hy-

pothesized that the kinematics of a point on the wing (defined by  $x_{ref}, y_{ref}$ ), that is, its induced angle  $\alpha_{eff} = \alpha + \arctan(\dot{\theta} y_{ref}/V)$ , can be used to reproduce the aerodynamic forces of the entire wing. As it is well-known, for airfoils it has been shown that the aerodynamics depends mainly on the effective angle of attack at  $x_{ref} = \frac{3}{4}c$  [14], an analogous representative point can be found along the span.

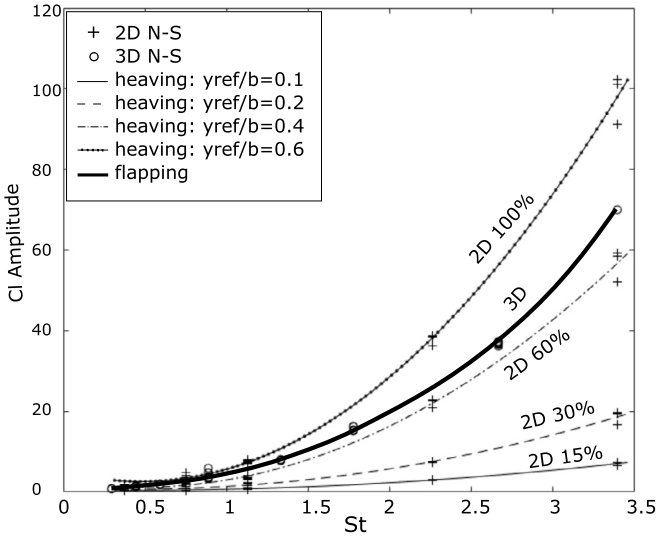
To start with, two-dimensional simulations of the wing's airfoils have been carried out, so that the movement of a flapping three-dimensional wing has been reproduced by the simulations of the airfoils that compose it, separately. In order to select the  $y_{ref}$ , related to the airfoil whose forces show a greater regression with the forces of the flapping wing. This can be interpreted as the "infinite wing" in heaving equivalent to the three-dimensional finite wing. The quality and characteristics of the mesh are equivalent, with a cell height of  $2 \cdot 10^{-4} m$  approximately.

Fig. 7 shows the amplitude of the lift coefficient of the simulated airfoils at different positions of the span ( $\frac{y_{ref}}{b}$ ), as a function of the Strouhal number, and the same results obtained for the three-dimensional flapping wing. Interestingly, the best fit is observed with the airfoil located at 70% of the wingspan, consequently,  $y_{ref} = 0.70b$ .

In what follows in this section, and for the sake of completeness, we show the aerodynamic coefficients obtained for a semi-wing, in "Unsteady Aerodynamic" reference frame (in the direction of  $\alpha_{eff}$  and perpendicular) for the last period of each simulation. The data is presented versus the effective angle of attack, as a function of the Strouhal [0.1, 0.84] and the static angle of attack (AoA) [-8, 20] deg. The coefficient of aerodynamic moment is measured at the center of the chord's root for convenience.



**Fig. 6.** Effective angle of attack of the surrogate airfoil. On CFD the aerodynamic forces ( $F$ ) depends on the induced velocity  $\alpha_{\text{eff}}$  which varies over the wing and time. In the ROM the aerodynamics is dominated by the effective angle of attack at an specific airfoil,  $y_{\text{ref}}$  at  $3/4$  chord. For pure flapping induced angle remains  $\alpha_{\text{eff}} = \alpha + \arctan(\dot{\theta}y_{\text{ref}}/V)$ .



**Fig. 7.** Simulated 2D lift coefficient amplitude during heaving cycle at various St and positions in the wing span ( $\frac{y_{\text{ref}}}{b}$ ). Thick line corresponds to 3D lift, which presents similar forces to approximately 70% airfoil.

**Lift coefficient (Fig. 8).** An approximately linear section with the effective angle is observed, up to approximately 40 [deg.]. By increasing the Strouhal, the induced angle is increased, which has a limit of 90 [deg.]. The lift coefficient decreases/increases rapidly at a positive/negative large effective angles of attack values respectively. It is observed that the static angle of attack has little influence on the peak values, even less for high Strouhal, since the angles induced by the wing are much bigger than the static one. In all the simulations, a strong time dependence of the effective angle has been observed, which justifies the use of memory-allowed models to identify them.

**Drag coefficient (Fig. 9).** It remains positive for most positions of the wing, however, this does not mean that the wing does not produce propulsion, since the projection of these coefficients on traditional aerodynamic axes provides negative resistance in certain cases. The resistance is approximately zero for null induced angles, since it is a flat plate in which case the fluid would be parallel to it. It should be noted that if the forces are projected on traditional aerodynamic axes, the resistance would be different from zero for a null static AoA. In general, the drag is a quadratic function of the induced angle. The discrepancies that exist between the values for a positive and negative angle may be due to the symmetry break between the upstroke and downstroke offered by the dihedral of the wing.

**Pitch moment coefficient (Fig. 10).** Shown with positive head-up, and even though it is also a non-linear function of the AoA (odd power), its time dependency is less noticeable.

Finally, the flow is also shown on Fig. 11. It can be observed how at intermediate Strouhal, a LEV detachment occurs, which influences the detachment of the Wingtip Vortex (WTV) creating complex structures downwards. While increasing Strouhal, also the trailing edge is detached, interfering with the own wing during the next stroke. It has been found that the LEV is detached at Strouhal higher than 0.3 at high angles of attack.

Fig. 12 compares the pressure contours during one stroke at Strouhal numbers 0.26 and 0.41. Notice that, in the latter the LEV detachment produces a low pressure gradient in the outer surface, providing an increase in lift. In the figure the scale of the colorbar has been kept to be able to compare. It can be seen that while in the case of low Strouhal the pressure contours remain smooth, in the case of higher Strouhal a large negative pressure gradient can be observed throughout the downstroke (Snapshots 1 and 4) produced by the detachment of the LEV, providing an increase in lift.

### 3. Reduced order model identification

As it has been aforementioned, CFD approaches are too computational expensive. Thus, a widely used and feasible approach in aerodynamics is the development of ROMs, with applications ranging from forces and moments estimation and control. In our application of ornithopters capable of performing maneuvers, high-precision models are strongly needed for the design and control. A suitable choice and well-known in the field is the Volterra model. In this section, the identification of a ROM based on Volterra theory fulfilling those requirements is proposed and validated.

#### 3.1. Model selection

System identification as data-driven modeling (see Fig. 13) can be performed by different methods. The Eigensystem Realization Algorithm (ERA), Autoregressive with exogenous input model (ARX) and Indicial functions models propose linear identifications. ERA method transform the Impulse response of the system in a state-space model with a predefined order. ARX method provides a general description of a dynamical system by including both input and output in their formulation. Regarding non linear methods, Volterra Series, NARMAX and block oriented methods have been used on aerodynamics identification. The choice of the Volterra model identified by a flapping training set (not stochastic or impulse) is justified as follows:

1. The first order Volterra series provide a simple model as a first iteration that fulfills the requirement of low computational load, being therefore suitable for a future onboard implementation. Moreover, this model can be easily enhanced with non-linear terms.
2. The noise of the training set signal will not be considerable since it is obtained by simulation. For this reason NARMA models are not considered.
3. The physical sense of the identified kernel is maintained, in analogy to Wagner's classical theory. For this reason, NARMAX models or neural networks are discarded.
4. A wide range of signal types can be used as a training set, while other methods are restricted to impulse or white noise signals. Simulating an impulse signal using CFD can lead to initialization problems that must be solved carefully.
5. However, according to the [48] reference, the Volterra models usually need a higher order than the ARX to reproduce similar accuracy in linear dynamics.

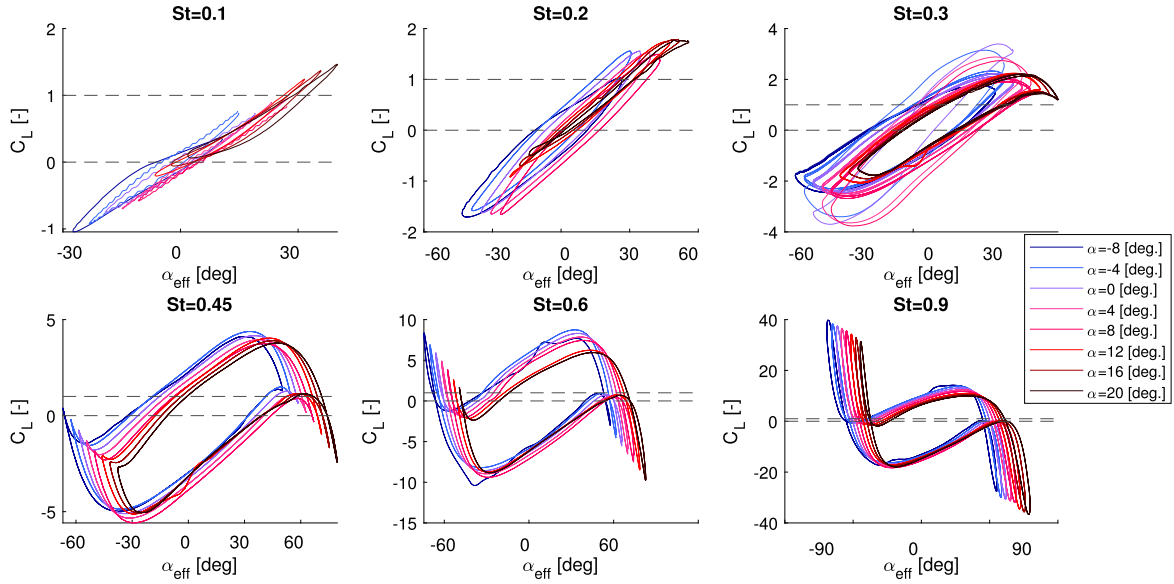


**Fig. 8.** Lift coefficient in Unsteady Aerodynamic reference frame. (For interpretation of the colors in the figure, the reader is referred to the web version of this article.)

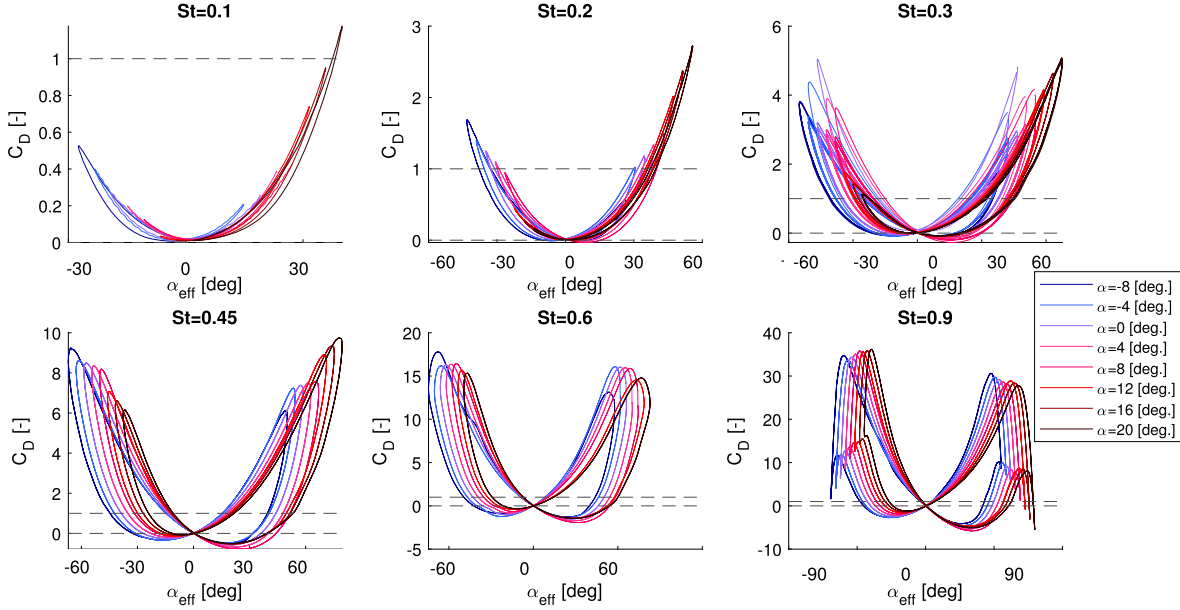


**Fig. 9.** Drag coefficient in Unsteady Aerodynamic reference frame. (For interpretation of the colors in the figure, the reader is referred to the web version of this article.)

Therefore, in this work we propose the identification of the first order Volterra model—suitable for a future onboard implementation—in order to be analyzed and compared with the classical methods, and current research is underway to explore enhanced versions of the model to capture non-linear effects, as e.g. the higher order Volterra or Hammerstein-Wiener models.

Let us start with the classical model of Wagner [14] which is based on small perturbations of an airfoil. The model for the aerodynamic lift coefficient can be described in the time domain through the Duhamel's superposition integral of steps responses [33] as

$$C_L(t) = -\frac{\pi b \ddot{h}}{V^2} + 2\pi \left[ w(0)\Phi(\tau) + \int_0^t \frac{1}{V} \frac{dw(t')}{dt'} \Phi(t-t') dt' \right], \quad (1)$$

where  $h$  is the heaving input that induces a vertical velocity  $w = \dot{h}$  at 3/4-chord, and  $\Phi$ , with  $\Phi(0) = 0.5$  and  $\Phi(\infty) = 1$ , is the well-known Wagner's step response. Thus, from (1) the use of the integral convolution with the induced angle of attack as state is physically justified in order to reproduce the unsteady aerodynamics of an airfoil. As mentioned, the lack of fulfillment of the hypotheses—mainly small perturbations—and the infinite memory need make this model useless in practice for prediction of aerodynamics in the range of interest.

On the other hand, the Volterra theory of nonlinear systems is very suitable for aerodynamics estimations because its causal and time-invariant fading memory characteristics. Its greatest potential lies in the ability to include system memory when computing outputs, as long as this memory is fading and weakly nonlinear

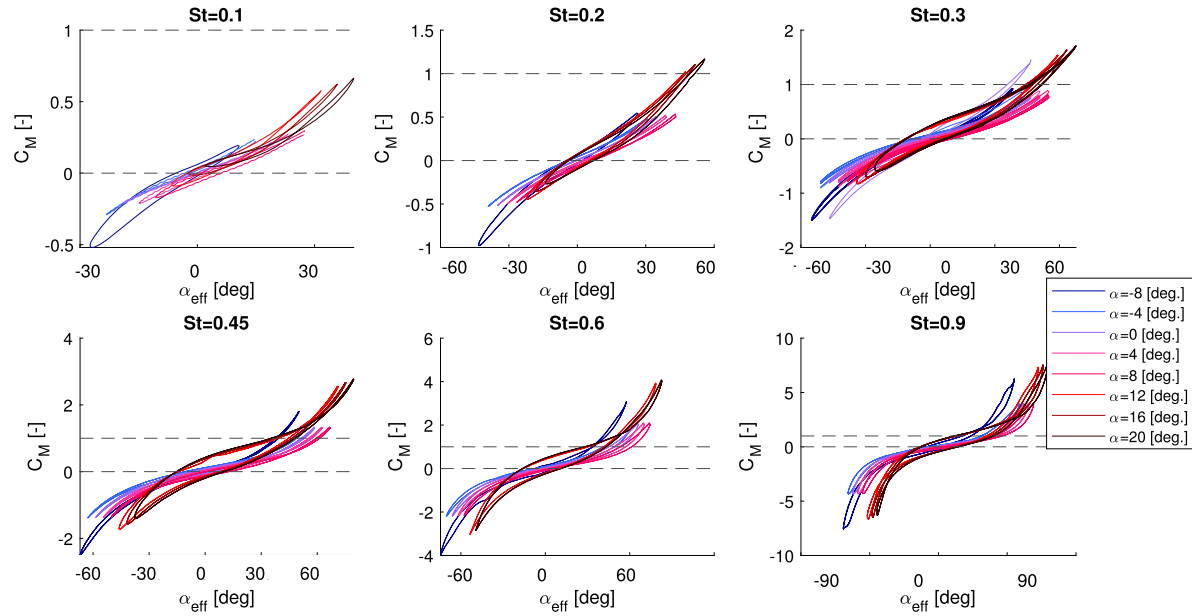


**Fig. 10.** Moment coefficient in Unsteady Aerodynamic reference frame. (For interpretation of the colors in the figure, the reader is referred to the web version of this article.)

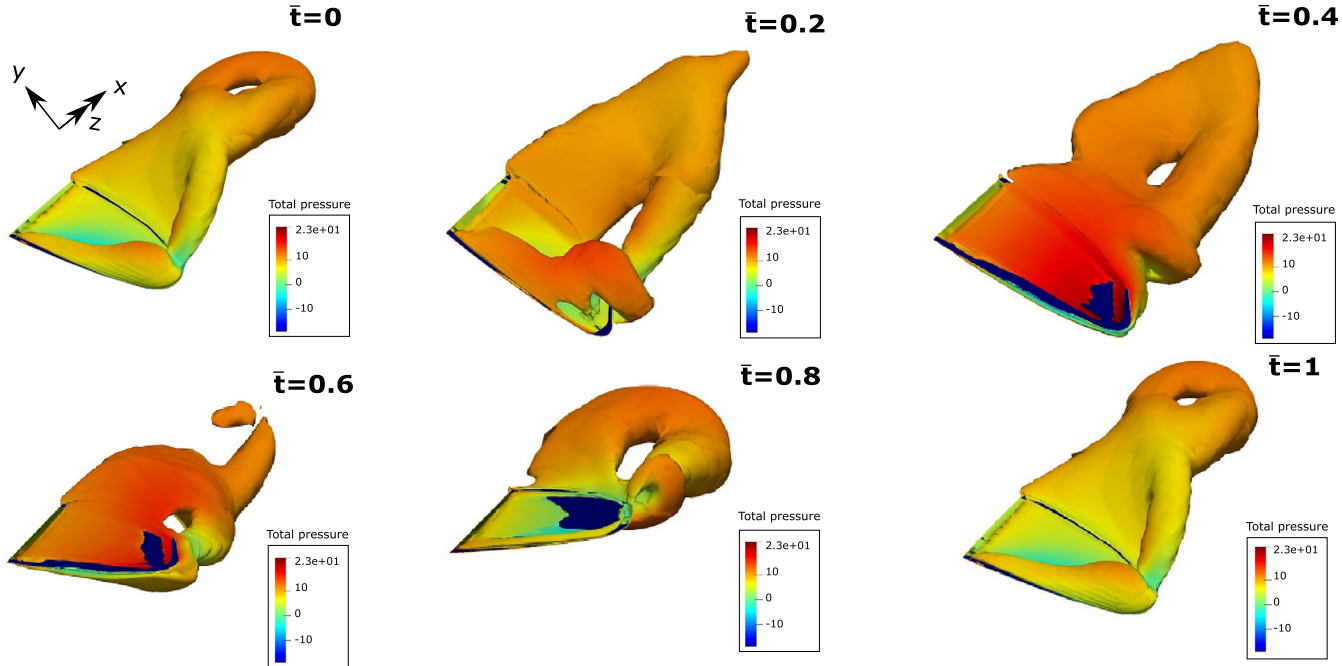


**Fig. 11.** Vorticity magnitude contours colored by total pressure at  $Re=10^5$  and  $St=0.3$ , at different points during a flap. From left to right, up to down: First, during downstroke, the effective angle of attack in the wing is maximum and the LEV is created and detached next to the WTV downwards. During upstroke, the WTV is detached but with less intensity, since the snapshots are from a positive static angle of attack. The resulting wake forms a figure-of-eight, reported in the classical analysis of birds flight [24], similar of those showed at reference [47]. (For interpretation of the colors in the figure, the reader is referred to the web version of this article.)

[49].<sup>1</sup> In particular, it is well known in the field of fluid mechanics that previous states play an important role in aerodynamics, fact that is mathematically posed through convolution-like integrals, and it has been corroborated in the simulation analysis made in the previous section. In fact, the Volterra series can be seen as the natural generalization of the convolution description of linear time-invariant operators for nonlinear systems [51]. Moreover, the

Volterra series applied to aerodynamic data can be understood as a numerical generalization of classical aerodynamic theories, being able to take into account any phenomenon produced by current or past system states. However, even though it has been extensively used to identify aerodynamic models of fixed-wing platforms, the application to flapping wing is actually very limited [44], becoming necessary for applications to gain more insights of relevant states and kernels that best suit their aerodynamics.

Thus, consider a single-input  $x(t)$  and single-output  $y(t)$  causal system, the bi-truncated Volterra series in continuous time can be written as

<sup>1</sup> For a detailed description of Volterra's theory we refer to interested readers e.g. [50] and references therein.

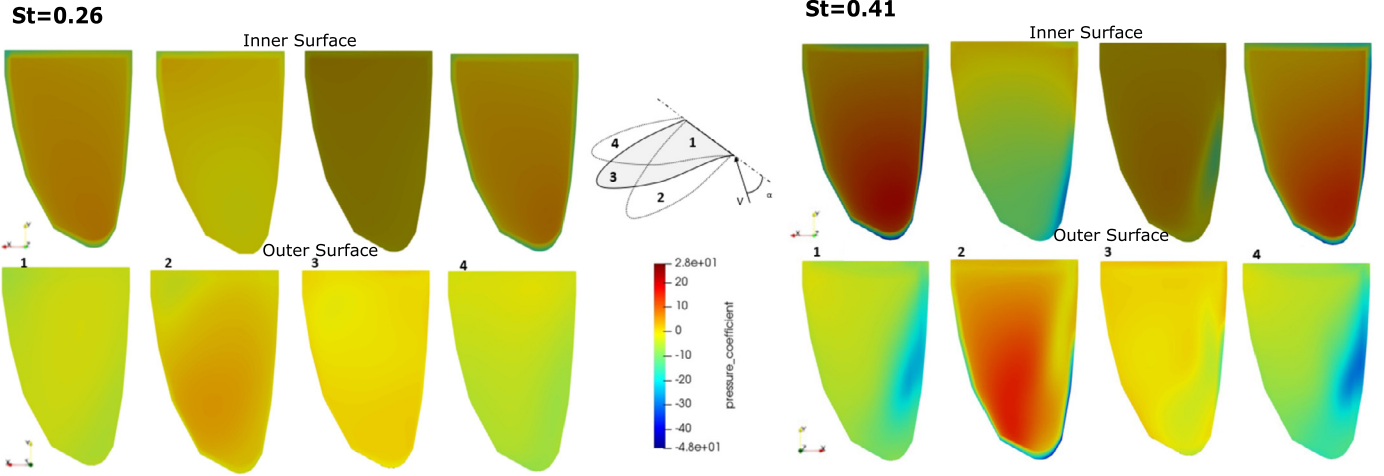


**Fig. 12.** Snapshots array of pressure contours of the wing over a complete flapping for two simulations cases. The Strouhal number remains at 0.26 and 0.41 on the left and right graphs. The upper and lower set of snapshots corresponds to inner and outer wing views. From left to right, snapshots during time: 1,3. Mean wing position, 2. Lower position, 4. Upper position. (For interpretation of the colors in the figure, the reader is referred to the web version of this article.)

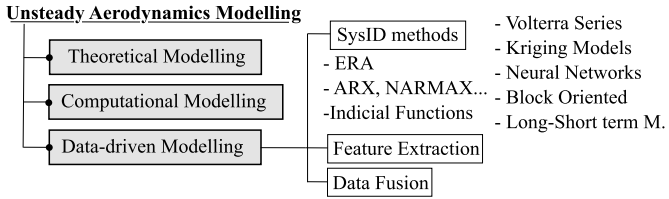


**Fig. 13.** Scheme of Unsteady Aerodynamics Modeling Methods. Data obtained from [32].

$$y(t) = y_0 + \int_{-\infty}^t \cdots \int H_p(t-t'_1, \dots, t-t'_p) \prod_{i=1}^p \{x(t'_i) dt'_i\}. \quad (2)$$

Motivated by (1), it is reasonable to consider a ROM with  $p = 1$  from (2) given by

$$y(t) = H_0 + \int_{-\infty}^t H_1(t-t')x(t') dt' \quad (3)$$

However, thus defined, the limits of the integral in (3) indicate that the response of the system at instant  $t$  depends on the entire history of the input. This definition makes it unapproachable in practice, for both simulations and applications, and unrealistic because the effect of previous states on current loads fades. For example, the effect of a vortex detached on the aerodynamic characteristics of the wing in an instant  $t$  would diminish due to the viscous effect of the fluid, and also the incident stream drag it downstream. Furthermore, it is well-known that the step response of the classical models converges to a stationary state eventually, and hence, the limit can be relaxed to obtain a finite-memory model, i.e. Finite Impulse Response (FIR). Taking all the above into account, it makes us suppose that a good choice for the Volterra series in discrete time from (3) becomes

$$y[\tau] = x[\tau - M]H[\tau] + \sum_{\sigma=\tau-M}^{\sigma=\tau} x[\sigma]\dot{H}[\tau - \sigma]\Delta t \quad (4)$$

where  $\Delta t$  is the time step with  $\tau$  and  $\sigma$  time indexes,  $x[\tau] = x(t)|_{t=\tau\Delta t}$  and  $y[\tau] = y(t)|_{t=\tau\Delta t}$  are the discrete input and output, respectively, and  $M$  denotes the number of past steps considered, i.e. memory. Note that the kernel  $H_1$  has been replaced by  $\dot{H}$  for

convenience. Finally, it only remains to define the output as lift coefficient  $y[\tau] = C_L[\tau]$  and the input as the non dimensional derivative of the effective angle of attack,  $x[\tau] = \dot{\alpha}_{eff}[\tau]$ , mainly due to their good agreement with CFD database. Recall that, the effective angle of attack induced at 3/4 chord at the  $y_{ref}$  chord becomes  $\alpha_{eff} = \alpha + \arctan(\dot{\theta}y_{ref}/V)$  for the surrogate heaving wing, where  $\theta$  is the flapping angle, and  $\dot{\alpha}_{eff} = \dot{\alpha}_{eff}b/V$  is its non-dimensional derivative. More details about the  $\alpha_{eff}$  are provided in section 2.2. Finally, notice the  $\arctan(\cdot)$  term because of the high-amplitude case considered, unlike in small perturbations approaches. The input signals used to simulate the CFD are the sinusoidal defined by  $\theta = \frac{A_f}{2} \sin(2\pi ft) - A_m$  and chirp functions,  $\theta = \frac{A_f}{2} \sin(\pi t^2) - A_m$ . The effective angle of attack they produce is shown on Fig. 14.

### 3.2. Identification

In the literature there are some techniques to identify the Volterra Models, which has been used in a variety of areas and applications. Regarding to identification method, the Cross-Correlation Method has been extensively used in signal processing and communications [52], [53], however the training set has different restrictions such as zero mean. The Impulse Unit Method become relevant in aerodynamics where Silva [39], [40] studied the application to unsteady aerodynamics of fixed wing platforms by experimental data. However the replication of an impulse change in AoA is challenging in CFD because of numerical instabilities. The identification process could be accelerate and optimized using basis functions in the field of aerodynamics, such as Orthonormal Basis Functions [54], however, a priori knowledge of the kernel it is needed. The direct identification has been used by Liu [44] to identify one maneuver of a flapping wing, where no information about kernels and method's details are provided, and it is chosen for the present method.

To test the ability of the proposed scheme, the Linear Volterra Model will be identified through the lift time series of the simulations. The derivative of the effective angle of attack in the position discussed above is chosen as the state, and the different coefficients of forces and moment as output. In the same kernel will be included all the phenomenon since the separation between circulatory and added mass effects has been shown arbitrary [38]. The model selected is shown in Equation (5), where  $\dot{H}$  is the kernel to identify, analogous to the Finite Impulse Response (FIR).

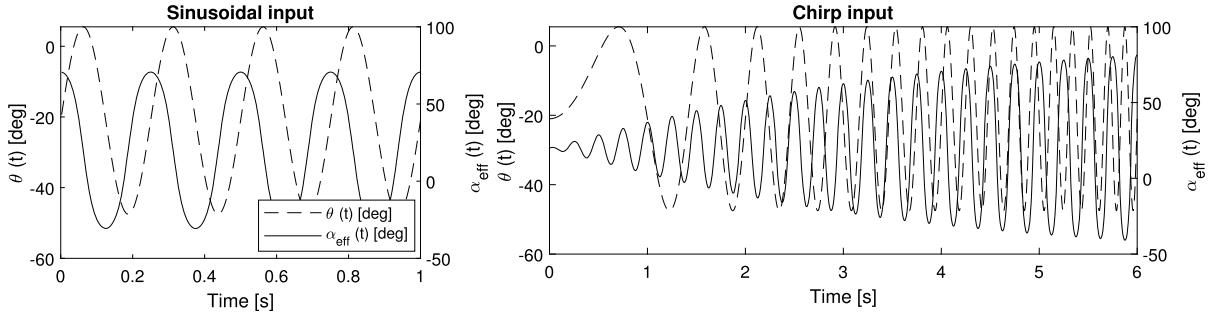


**Fig. 14.** Input signals of the training set, flapping angle and the effective angle of attack they produce. Note that while the flapping amplitude is constant by construction, the  $\alpha_{eff}$  they produce depends on velocity and frequency. The signals showed corresponds to a Velocity of 4 m/s,  $\alpha = 20$  deg and  $f = 4$ Hz for sinusoidal.

$$C_L[\tau] = \alpha_{eff}[\tau - M]\mathcal{H}[\tau] + \sum_{\tau-M}^{\tau-1} \dot{\alpha}_{eff}[\sigma]\dot{\mathcal{H}}[\tau - \sigma]d\sigma. \quad (5)$$

By carrying out the necessary operations, the model become a linear system such as  $A\mathbb{H} = B$ , which can be identified by various methods. If  $N$  is the length of the state and output ( $B$ ) time series, the matrix  $A$  would have dimensions  $(N-M \times M+1)$ , and it will multiply if the Nonlinear Volterra Model is chosen. However, nowadays computing power is rarely the main problem. In this case the main difficulty comes from the formulation of the identification method itself. This is badly conditioned by definition so the rank of the matrix is low. Therefore, direct identification using least squares is not feasible, and regularization techniques are needed.

$$A = \begin{bmatrix} \alpha_{eff}[1] & \dot{\alpha}_{eff}[1] & \dot{\alpha}_{eff}[2] & \dots & \dot{\alpha}_{eff}[M] \\ \alpha_{eff}[2] & \dot{\alpha}_{eff}[2] & \dot{\alpha}_{eff}[3] & \dots & \dot{\alpha}_{eff}[M+1] \\ \vdots & & & & \vdots \\ \alpha_{eff}[N-M] & \dot{\alpha}_{eff}[N-M] & \dot{\alpha}_{eff}[N-M+1] & \dots & \dot{\alpha}_{eff}[N-1] \end{bmatrix} \quad (6)$$

$$\mathbb{H} = [\mathcal{H} \quad \dot{\mathcal{H}}[M] \quad \dot{\mathcal{H}}[M-1] \quad \dots \quad \dot{\mathcal{H}}[1]]^T \quad (7)$$

$$B = [C_L(M+1) \quad \dots \quad C_L(N)]^T \quad (8)$$

To solve this, Ridge Regularization is proposed as a method to avoid over fitting due to multicollinearity. Although others have been used (Moore-Penrose Semi-inverse between them) this is the one that has led to the best results. The identification is defined as follows, where  $\lambda$  is the regularization parameter selected taking into account the lowest appreciable eigenvalue of  $A$  matrix, and  $I$  is the identity matrix of dimension  $(M+1)$ .

$$\mathbb{H} = (A^T A + \lambda I)^{-1} A^T B \quad (9)$$

After some tests, it has been obtained that the step response stabilizes after 600 time steps at  $dt = 1/1200$ , so the memory is set at approximately 0.5 seconds. The computation time for an identification set of a time series with 24000 points is less than 5 seconds. The kernels have been identified for sets of simulations at different mean angles of attack and frequencies, keeping the upstream velocity constant. For each velocity, a kernel has been obtained, Fig. 15, valid for the entire range of angle of attack in study. Since it has been observed that the angle induced by the flapping frequency is greater than the geometric angle of attack, it has been assumed that the kernel will only depend on the effective angle of attack, which includes the geometric one. It is worth mentioning, a dependency of the kernel has been observed with the fluid inlet velocity.

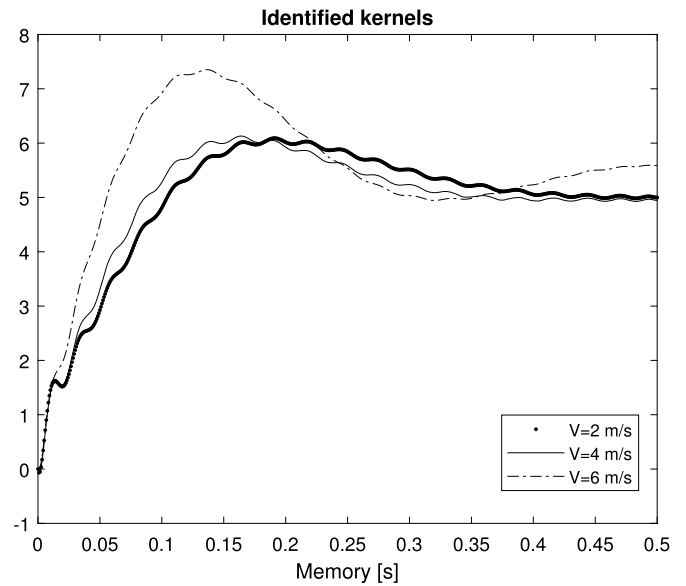


**Fig. 15.** Reconstructed step response  $\int_0^{Mdt} \dot{\mathcal{H}} dt + \mathcal{H}$ . It is observed how the response reaches a stationary value lower than the theoretical one ( $2\pi$ ) for all speeds.

### 3.3. Analysis

One of the main problems with the identification of the Volterra Model is the loss of physical meaning that occurs with the identification of the kernel. However, taking the frequency response of the Theodorsen model as a reference (Note that Wagner's model function  $\Phi(\tau)$  in frequency domain corresponds to Theodorsen's model function  $C(\bar{s})$ ), the differences can be quantitatively analyzed and associated with aerodynamic effects. The Theodorsen's Model is shown in Equations (10) and (11) for  $\alpha_{eff}$  and  $\dot{\alpha}_{eff}$  as input respectively.

Figs. 16 and 17 show the frequency response of the data obtained from the CFD simulations, the Theodorsen model, and the Jones aspect ratio correction as a function of the effective angle and its derivative, where  $\bar{s} = ik$  is the non-dimensional Laplace variable.

$$\mathcal{L}\left[\frac{C_L}{\alpha_{eff}}\right] = \pi\bar{s} + 2\pi C(\bar{s}) \quad (10)$$

$$\mathcal{L}\left[\frac{\dot{C}_L}{\dot{\alpha}_{eff}}\right] = \pi + 2\pi \frac{C(\bar{s})}{\bar{s}} \quad (11)$$

$$C(\bar{s}) = \frac{0.5\bar{s}^2 + 0.2808\bar{s} + 0.01365}{\bar{s}^2 + 0.3455\bar{s} + 0.01365} \quad (12)$$

The input for the 3D simulations has been chosen at 70% of span, since it has been demonstrated that is the surrogate airfoil.

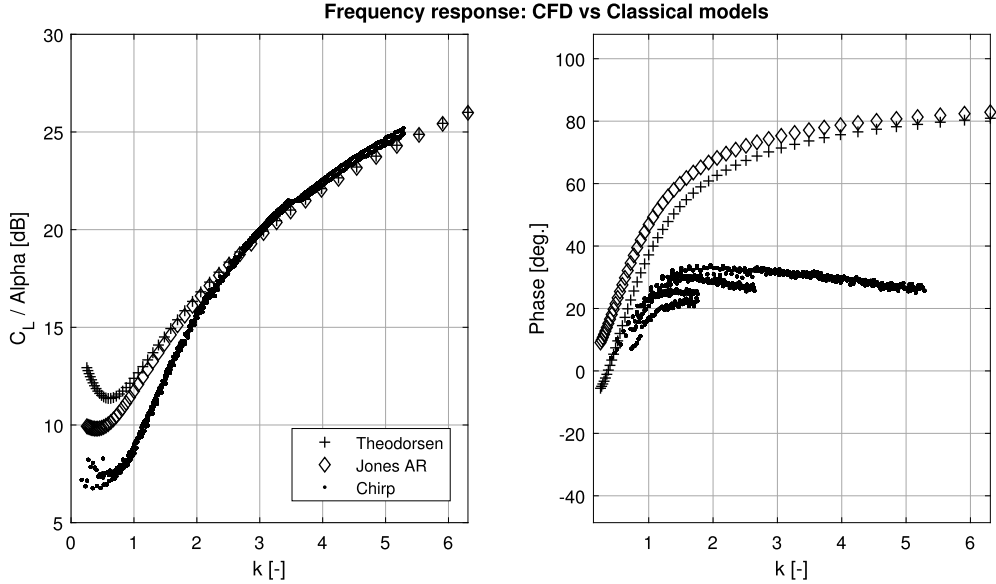


**Fig. 16.** Frequency response of Theodorsen (Plus markers), Jones correction (diamond markers) and CFD simulations (dot markers) lift coefficient with  $\alpha_{eff}$  as an input.

Regarding the magnitude in Fig. 16, it can be observed that for low and moderate reduced frequencies ( $k < 2$ ), the classical models underestimate the lift force. This range is influenced, according to Theodorsen, by the circulatory forces in the airfoil, which are diminished by the effect of the aspect ratio. The WTV in flapping is generally higher than in heaving, so the force will be much less than predicted. In the high frequency zone ( $k > 3$ ) an increase in lift is observed compared to that expected. This hyper-lift phenomenon has been pointed out by several authors as the cause of LEV detachment. Regarding to phase, in inviscid theory, a positive phase which tends to 90 deg is found in most reduced frequencies, showing that the influence of the first derivative is dominant, except for low frequencies. In the classical Theodorsen's model it can be observed that the forces due to the apparent mass gain relevance when the frequency of oscillation of the airfoil increases, producing a phase advance with respect to the effective angle of 90 degrees in the upper frequency limit, since it is directly proportional to airfoil acceleration. On the other hand, the magnitude is diminished for large frequencies, and the limit of the transfer function being 0.5 for large frequencies, in concordance to Wagner instantaneous lift. For small frequency values, the contribution of forces due to the circulatory characteristics of the airfoil becomes relevant.

However, a very remarkable fact is that the simulations tend to a lower value, around 30-45 degrees depending on the free stream velocity (The different lines seen in CFD correspond to simulations at different speeds, which when simulated up to a specific frequency, they reach different Strouhal.). This may mean that the influence of the angle and its first derivative remain equivalent. Taking into account the recent study by Taha [38], where it is shown how the circulation actually has a phase that tends to -45 degrees, as opposed to the controversially defined Theodorsen circulatory force that would tend to 0, it may be suspected that there are mechanisms not taken into account in the inviscid theory that cause the phase to tend to a value less than 90 degrees under certain conditions. Due to this, it is not possible to identify a rational transfer function through our data as proposed by [33], since rational functions phase tends to a multiple of 90 deg, which multiplication factor depends on the order of numerator and denominator of the transfer function.

Regarding the mean values of the aerodynamic forces, the CFD results have been compared to those of classical models. They are

**Table 3**

NMSE of CFD and Volterra Model frequency response, in magnitude and angle. The maximum error is 6.6% in magnitude and 3.4% in phase. Note that  $\Theta$  and  $\hat{\Theta}$  are the values from CFD and estimated from the identified model respectively.

$NMSE = \frac{E[(\Theta - \hat{\Theta})^2]}{E[\Theta \hat{\Theta}]}$	$V = 2$ m/s	$V = 4$ m/s	$V = 6$ m/s
$ \mathcal{L} \frac{ C_L }{ \alpha_{eff} } $	0.015	0.006	0.066
$\angle \mathcal{L} \frac{ C_L }{ \alpha_{eff} }$	0.034	0.019	0.018

shown as a function of the reduced frequency  $k$ , and the aerodynamic angle of attack  $\alpha$ , from CFD simulations, on Figs. 18a and 18c, and from analytical models on Figs. 18b and 18d. A great dependence with  $\alpha$  is observed. The mean  $C_L$  during a cycle is generally lower in CFD than that of the Wagner model, due to the WTV effect as explained before. Besides that, at small angles of attack and low frequencies the CFD result is negative. This may be because the vortices generated during the cycle interfere with the circulatory effects that occur at small angles of attack. In general, both increase with the angle of attack, and decrease slightly with the Strouhal.

The average drag coefficient, or propulsion if negative, has been compared in the figure with that obtained by Feria [18] using the Vortical Impulse theory, for small induced angles and therefore small amplitudes. While this theory provides a monotonic relation with reduced frequency and little dependence on the mean angle of attack, the CFD simulations predicts a highly non-linear map, with dependence on  $|\alpha|$ . Also, the maximum thrust in the study range is at angles around 8 deg. and maximum reduced frequency. Also, in general, the propulsion predicted by CFD is lower.

### 3.4. Verification

The identified kernels have been verified using training chirp time series dataset. An example of the signal is provided in Fig. 19. The identified and CFD models are compared in frequency response in Figs. 20 and 21, where Normalized Mean Squared Error is shown in Table 3.

It can be seen how the identified Volterra model correctly reproduces the frequency response of the system. The phase and magnitude is captured with great precision, however the amplitude at a very small Strouhal has a greater error.

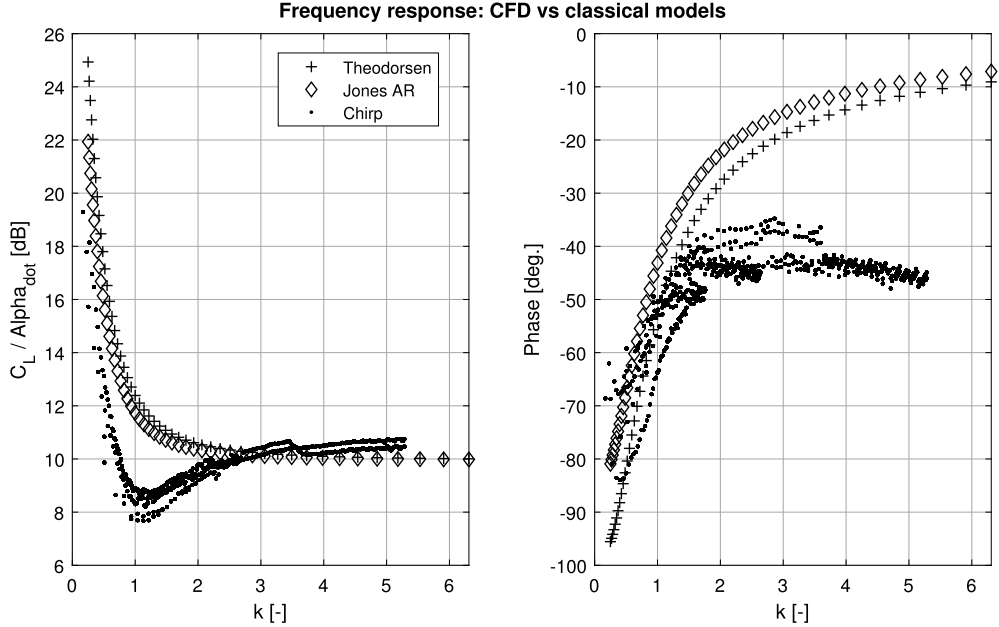


**Fig. 17.** Frequency response of Theodorsen (Plus markers), Jones correction (diamond markers) and CFD simulations (dot markers) lift coefficient with  $\dot{\alpha}_{\text{eff}}$  as an input.

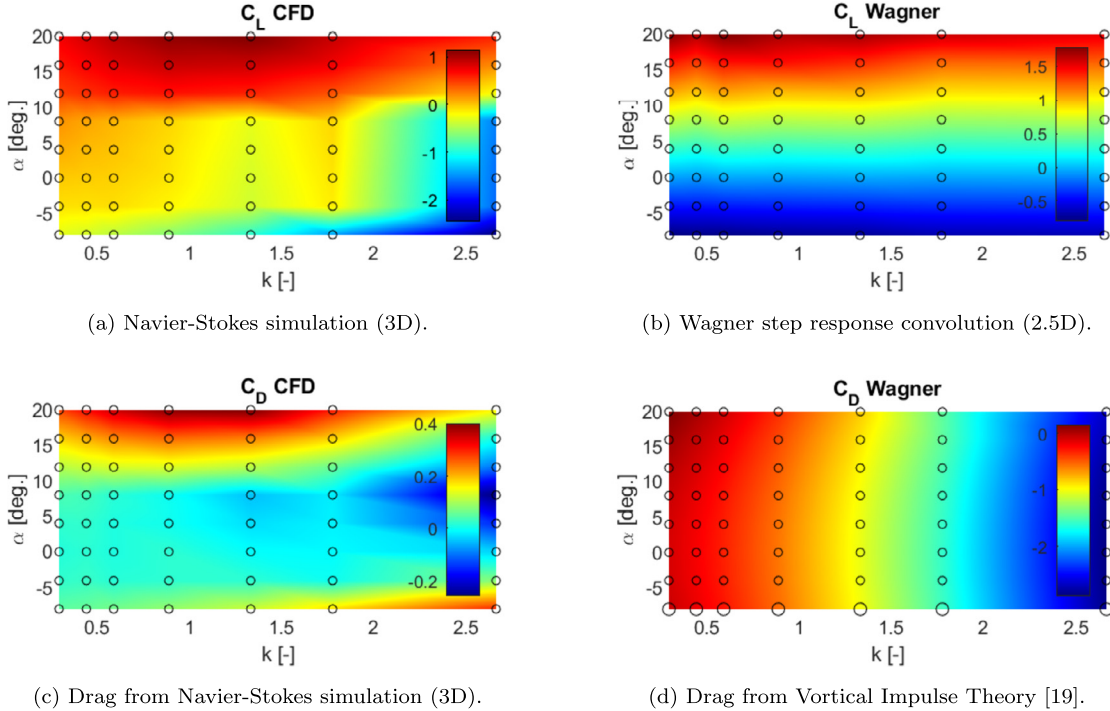


**Fig. 18.** Mean lift and drag coefficient in function of reduced frequency  $k$ , and mean angle of attack  $\alpha$  (aerodynamic reference frame), from CFD on left side, and from theoretical models on right side. The colormaps has been interpolated from the simulated points (Black circles). Note that figures have different colorbar range. (For interpretation of the colors in the figure, the reader is referred to the web version of this article.)

#### 4. Flight experiments: validation

In order to obtain estimates of the aerodynamic forces of the ornithopter, indoor open-loop flapping flights experiments have been performed at different constant frequency, in the GRVC<sup>2</sup> facilities. Fig. 22 represents a block diagram resume of the proposed approach to validate the identified Volterra Model by flight experiments.

The total forces and moments are reconstructed by the measurements of a precise Motion Capture System (MCS), shown in Fig. 23, which provides position and attitude with a frequency of 120 [Hz]. Redundant active markers fixed in the ornithopter are used, as shown in Fig. 24 and the system is calibrated in such a way that a precision of 2 millimeter is reached at the position of the markers throughout the flight. The initial conditions for angle of attack, speed, and tail position both in pitch and roll, are such that the ornithopter is intended to start flight under trim conditions to promote sustained two-dimensional flight, and are

<sup>2</sup> Group of Robotics, Vision and Control Lab, University of Seville.

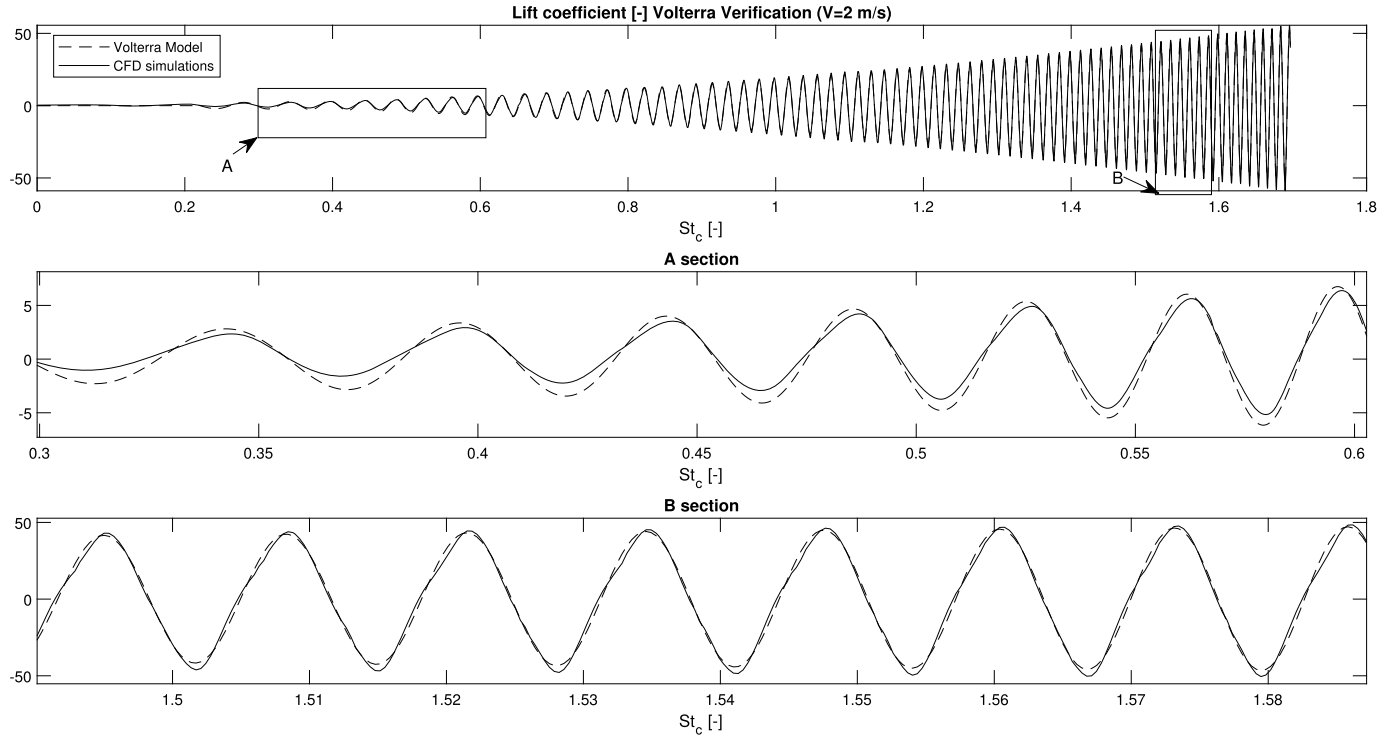


**Fig. 19.** Lift coefficient of a chirp maneuver at  $V = 2 \text{ m/s}$  and  $\alpha = 20 \text{ deg}$  in function of the Strouhal number. Note that since the frequency of the flapping varies linearly with time on chirp maneuver, the Strouhal number is proportional to the time. Second and third figures are the pieces A and B of the signal (Low and high Strouhal respectively).

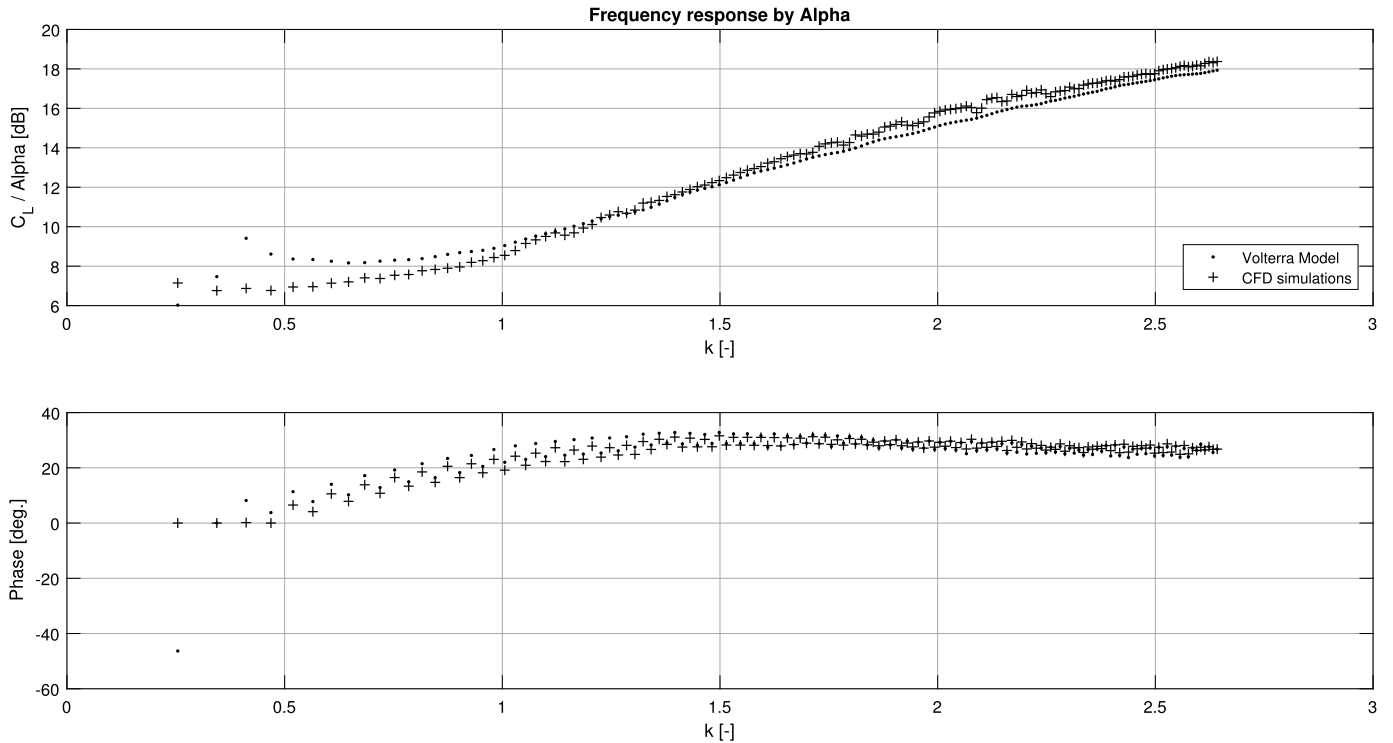


**Fig. 20.** Frequency response of CFD simulations and Identified Volterra Model:  $|L\left[\frac{C_L}{\alpha_{eff}}\right]| \text{ [dB]}$  and  $\angle L\left[\frac{C_L}{\alpha_{eff}}\right] \text{ [deg.]}$ .

estimated for each frequency manually. The flapping frequency remains constant at each experiment, and the velocity and angle of attack oscillates in the flight around the equilibrium position because of the absence of control. It has been proved that the flight is preformed sufficiently in a vertical plane after trim to

assume that lateral forces can be neglected. To obtain the forces and moments, a two-dimensional movement is assumed, so the two-dimensional dynamic equations of flight are used. The inertia model of the ornithopter is shown in Table 4, which has been calculated by high accurate CAD (Computer Aided Design) model.

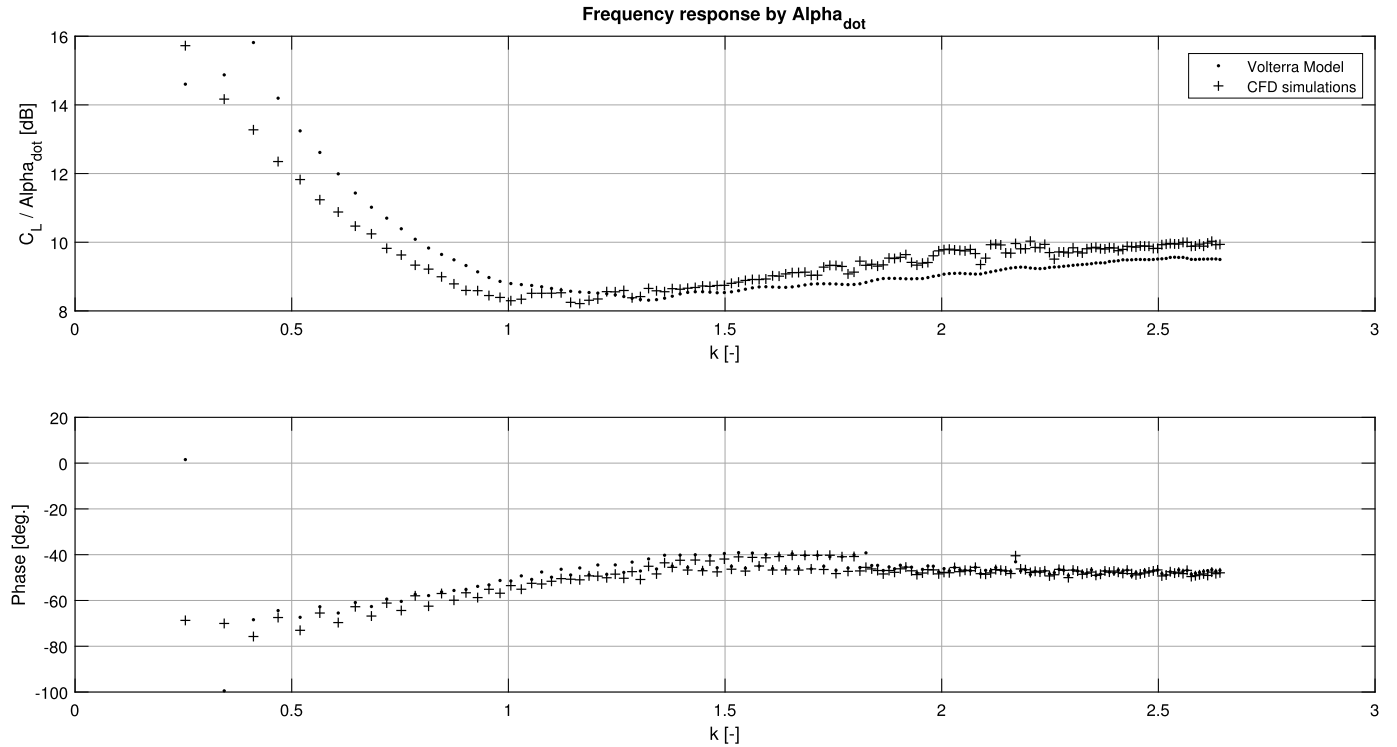


**Fig. 21.** Frequency response of CFD simulations and Identified Volterra Model:  $|C_L / \alpha_{eff}|$  [dB] and  $\angle C_L / \alpha_{eff}$  [deg].

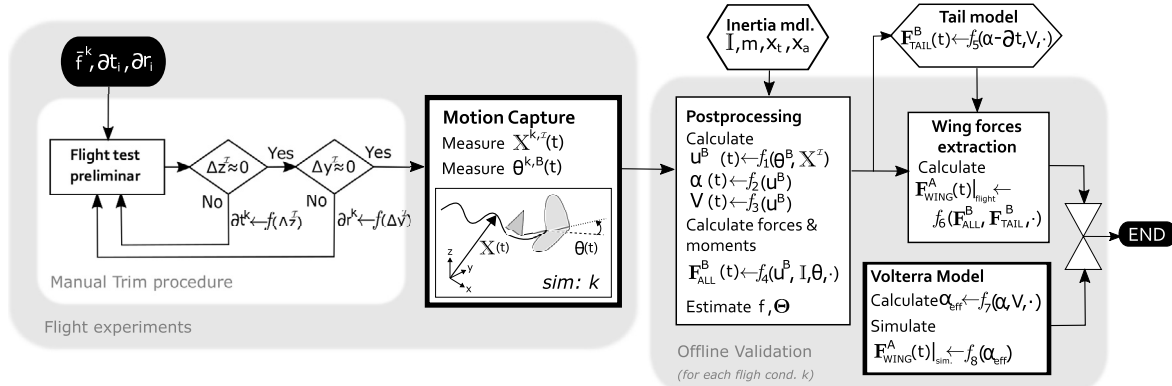


**Fig. 22.** Proposed methodology for Validation.

**Table 4**  
Inertia model of the ornithopters test case.

Total mass	0.635 [kg]
$I_{yy}$	0.028 [kg·m <sup>2</sup> ]
$x_a$	0.013 [m]
$x_t$	0.434 [m]

The measurement of the position of the markers is post-processed to obtain the attitude and force estimates through equations  $f_{1-4}$  which corresponds to Equations (13), (14) and  $f_3 : V = \sqrt{u^2 + w^2}$ . The maneuver is simulated by the identified Volterra model ( $f_8$ ) using the raw measured effective angle of attack and velocity from flight ( $f_7$ ) in order to be compared to aerodynamic forces reconstructed from flight. (See Fig. 25.)

The dynamic equations that allow to extract the lift, moment and drag (L, M, D) produced by the wing in position A previously described, are shown below. First the position measured in inertial reference frame ( $x^h z^h$ ) is derived and transformed to body refer-

ence frame (b). Then total forces and moment ( $F_x, F_z, M_y$ ) in body frame are constructed by the body accelerations and pitch (14), and tail influence is subtracted in (16).

$$\begin{bmatrix} u^b \\ w^b \end{bmatrix} = \begin{bmatrix} \cos(\theta) & -\sin(\theta) \\ \sin(\theta) & \cos(\theta) \end{bmatrix} \begin{bmatrix} \dot{x}^h \\ \dot{z}^h \end{bmatrix} \quad (13)$$

$$\begin{aligned} F_x &= \dot{m}u + mg \sin(\theta) + mw\dot{\theta} \\ F_z &= \dot{m}w - mg \cos(\theta) - mu\dot{\theta} \\ M_y &= I_{yy}\ddot{\theta} \end{aligned} \quad (14)$$

For this, it is necessary to implement an aerodynamic model of the bioinspired tail ( $L_t, D_t$ ), which has been obtained through experiments in a tunnel of wind, and depends on the free stream velocity and relative angle of attack. Recall that  $\alpha = \arctan(\frac{w}{u})$  and more information about this model used in the scheme in ( $f_5$ ) can be found in [55].

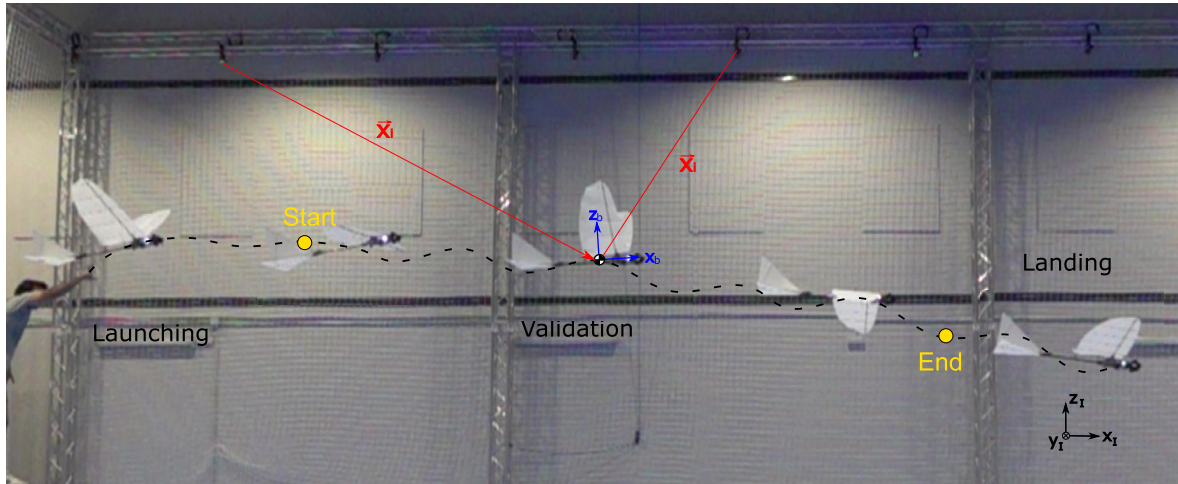


**Fig. 23.** Typical path of a flight experiment with snapshots. The ornithopter is launched by hand, which disturbs the flight in the first moments. The Motion Capture system measures its trajectory and attitude throughout the flight. Useful data for force reconstruction begins from the time the flight stabilizes (Start point) until seconds before landing (End point).

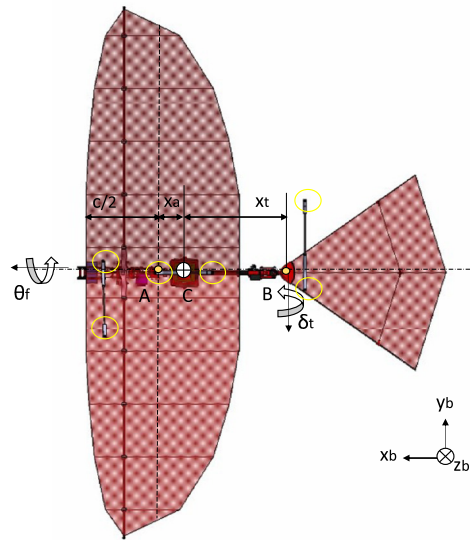


**Fig. 24.** Schematic representation of the bird model. Points A, B and C represents the center of the root chord wing, the hinge point of the tail rotation, and the center of mass, which are measured to implement in the dynamic model. The active markers positions are highlighted.

$$\begin{bmatrix} L \\ D \\ M \end{bmatrix} = \begin{bmatrix} \sin(\alpha) & -\cos(\alpha) & 0 \\ -\cos(\alpha) & -\sin(\alpha) & 0 \\ 0 & x_a & 1 \end{bmatrix} \begin{bmatrix} F_x \\ F_z \\ M_y \end{bmatrix} + \begin{bmatrix} -L_t(\alpha - \delta_t, V) \\ -D_t(\alpha - \delta_t, V) \\ -M_t(\alpha - \delta_t, V) + M'_t \end{bmatrix} \quad (15)$$

$$M'_t = (x_a + x_t)(L_t \cos(\alpha) + D_t \sin(\alpha)) \quad (16)$$

Once the data from flight is post-processed, the reconstructed model inputs, such as free stream speed, angle of attack and frequency are used to simulate the same maneuver by the aerodynamic model. The memory is adapted to flight time step which is ten times higher. In Fig. 26 can be found various validation sets from flight compared to our model (Volterra Model) and the classical model of Theodorsen. The Volterra model reproduces well the amplitude and mean of the experiments, while Theodorsen overestimate lift amplitude and in lower level, mean lift.

Note that while the flapping frequency is selected a priori by flapping actuator commanded power, is measured in flight since

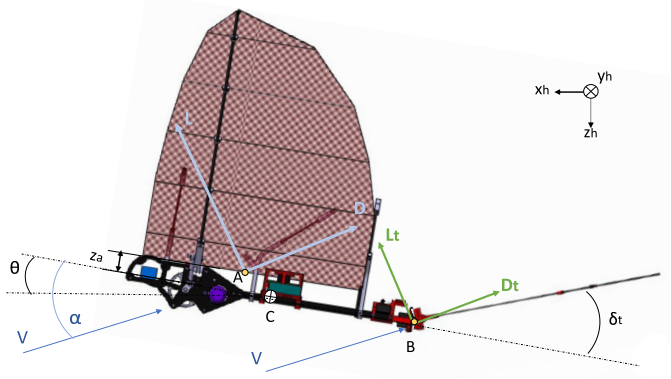


**Fig. 25.** Forces and moments considered in the ornithopters flight. Note that the angle of attack of the tails is diminished by the tail deflection.

**Table 5**

NMSE of ROM and Wagner Model respect flight data at different k values, corresponding to Fig. 26 b-d. The identified model obtained a higher precision than the Wagner model, being the mean error values 7% and 40% respectively.

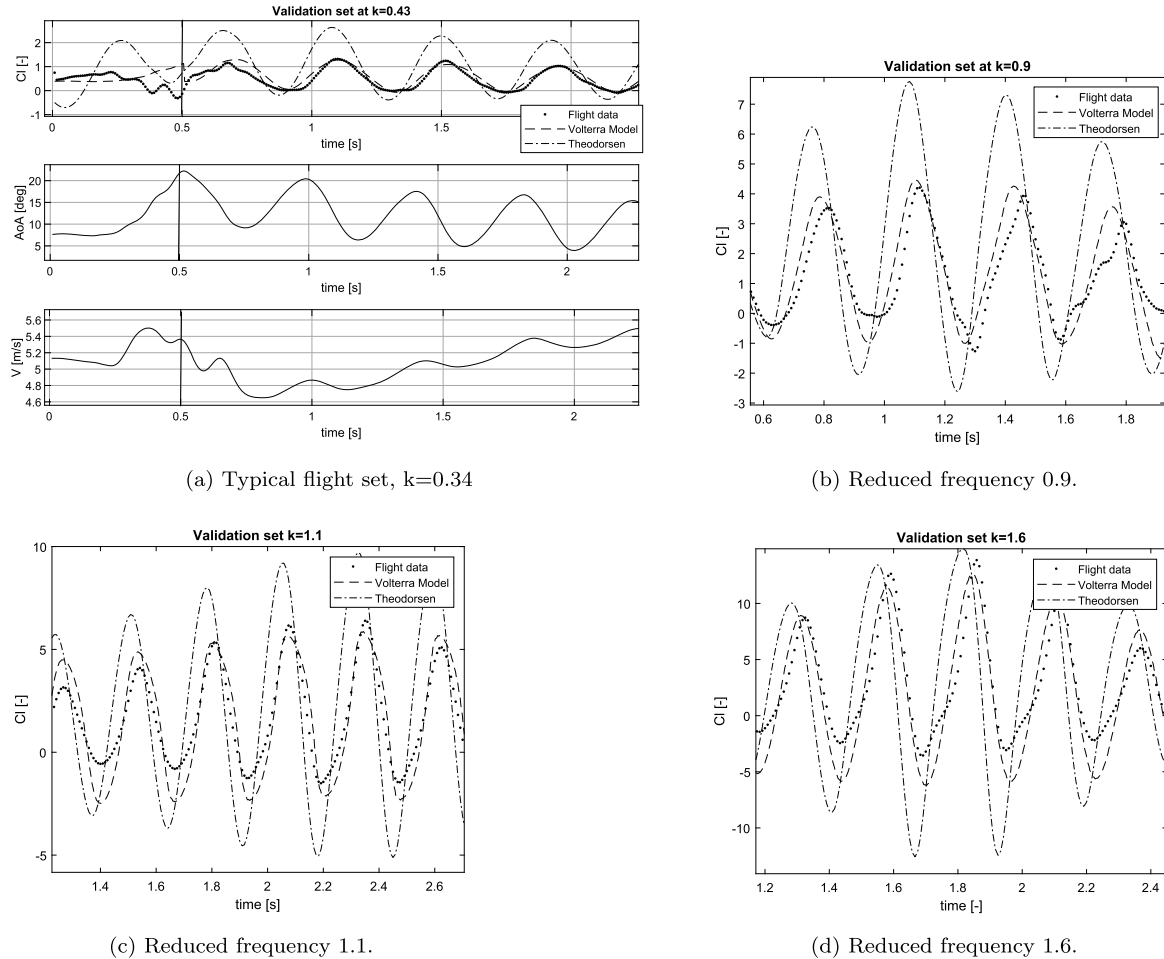
$NMSE = \frac{E[(\Theta - \hat{\Theta})^2]}{E[\Theta^2]}$	k=0.9	k=1.1	k=1.6	mean
ROM – Volterra	0.025	0.066	0.144	<b>0.078</b>
Wagner	0.442	0.372	0.359	<b>0.391</b>

depends on many variables like batteries level or environment. However, wing stroke position, which could provide the phase between the effective angle of attack and aerodynamic forces is not measured yet, so the phase is selected for best estimates.

## 5. Discussion and limitations

Regarding the effort versus the advantages of the approach, the reduced order model obtained by following the proposed methodology we achieve a reduction in computing time of the order of  $2 \cdot 10^4$  (CFD versus ROM computing time). Thanks to this, we envision that this ROM could be used onboard, which is its ultimate goal, to be able to implement optimization schemes and/or complex model-based controls, that with the use of CFD models would be unfeasible.

The sources of uncertainty are diverse. First, the wing is slightly flexible, and this has not been modeled in the present study,

Fig. 26. Validation set at different  $k$ .

mainly due to the computational times required to solve the FSI problem and the difficulty to obtain experimental data allowing us to discriminate the flexibility. Thus, the aeroelastic effect is currently under investigation and it will be part of a future work in this research line, to completely characterize and validate the physical mechanisms with in-flight data. On the other hand, the inertia model used to reconstruct the aerodynamic forces from the flight experiments is considered constant, and the experimental data show that the change in inertia due to the beating of the wings can be considerable outside the plane of symmetry. Therefore, current work is also in the direction of identifying the lateral model to be able to follow the proposed methodology. Other sources of error not considered can come from the inaccuracies of the tracking system (MCS), either due to the loss of markers or the uncertainty of their location, in addition to the wind if the experiments are carried out outdoors. However, the total error committed is considered acceptable for a stable flight indoors, as can be seen in Table 5, where the maximum and mean error of the identified ROM is 14 and 7 percent, respectively.

The ROM model has been identified in the range of large amplitudes of interest. As it only contains the first Volterra kernel, it may not be valid for highly non-stationary flows or for very large frequencies involving effective angles outside the identification range. Therefore it should be used with caution within its limits of use. Also it has been observed that the kernel remains constant after some time with a certain smooth undulation. However, it has not been possible to determine yet whether they are due to the shedding of vortices that takes place during flapping or other phenomena. In a future iteration where the non-linear model

will be identified, more information will be available to discuss it. It is also worth mentioning that the kernel memory size must be selected carefully. In our case, it has been selected in such a way that the slope of the kernel is practically zero after a certain time, so that increasing the memory size after this time would not have any improvement in precision. This is possible as the aerodynamic effects fade due to the viscosity of the fluid, and therefore it cannot be extrapolated to any identification of another phenomenon through Volterra series without further and dedicated experimentation.

Although it has not been included in the model, high-pitching rates of the ornithopter cause additional loads in the wing. However, we presume this effect could be modeled by our ROM, to a good approximation, if it is included in the effective angle of attack through a simple formula:  $\alpha_{eff}^q = \alpha_{eff} + qx_w/V$  where  $q$  is the pitch velocity and  $x_w$  is the distance from 3/4 of the chord to gravity center. On the other hand, the lateral movements of the ornithopter could induce speeds in the wing different from those taken into account in the current longitudinal model, so it is expected that the forces reproduced by the model will not be precise in large lateral movements. In addition, it should be said that for a future identification of drag the  $\alpha_{eff}^2$  could be used as input in the identification procedure, as proposed in [56].

A final comment is that some difficulty has been encountered when maintaining a stable flight in a limited space such as the testbed, for which the correct launch near a trim point has been crucial to obtain proper data that could validate the proposed model.

## 6. Conclusions and future work

The aerodynamic forces and moments produced by an ornithopter elliptical wing in forward flight performing high amplitude flapping at intermediate-range Reynolds has been simulated by unsteady CFD computations. The results has been analyzed quantitatively and qualitatively using time series and graphical post-processing tools respectively. The Leading Edge Vortex is detached after Strouhal 0.3 is reached during middle down stroke. In addition, it has been compared in frequency domain with the classical model of Theodorsen for a airfoil. For that, bi-dimensional CFD simulations have been performed where is shown that the three dimensional wing fits better with the airfoil located at approximately 70 percent of the semi span, performing heaving with the corresponding amplitude. So regarding to modeling, the effective angle of attack located at this position span wise and three quarters chord in chord-wise direction is chosen as input for the aerodynamic model. It has been found that the magnitude is overestimated by classical models at low reduced frequencies. The phase tends to approximately 30 degrees instead of 90 degrees of the Theodorsen's model.

The CFD simulations has been identified by a Volterra Model using the linear kernel, where a memory of 0.5 second has been found sufficient. A Ridge regression has been found the best fit. Finally, the identified model is validated through aerodynamic forces reconstructed from flight data positions and attitude measures by a high fidelity Motion Capture System. The model is capable to be used to simulate the aerodynamic forces acting on an ellipsoidal wing ornithopter performing high amplitude flapping at high angles of attack and intermediate-range Reynolds number, for any time series of effective angle of attack (including flapping frequency, incident velocity and mean angle of attack). The computation time of the model is very low and so, it could be used to in-flight estimation.

Current research is underway of measuring the position of the wing in flight to validate the phase between effective angle of attack and the aerodynamic forces and moments. This could be done using MCS and placing markers on the wing to become an skeleton instead of rigid body. Regarding to future work, a similar conclusion than other ornithopter researchers has been reached: the state of the art of ornithopters aerodynamics and flight mechanisms is much less than the insects robots. There are several topics that still need to be studied, like the lateral aerodynamics in flight and optimum kinematics of birds wings, among others.

## Declaration of competing interest

The authors declare that they have no known competing financial interests or personal relationships that could have appeared to influence the work reported in this paper.

## Acknowledgement

The authors acknowledge support from the European Project GRIFFIN ERC Advanced Grant 2017, Action 788247.

## References

- [1] U. Pesavento, Z. Wang, Flapping wing flight can save aerodynamic power compared to steady flight, *Phys. Rev. Lett.* 103 (2009) 118102, <https://doi.org/10.1103/PhysRevLett.103.118102>.
- [2] W. Send, M. Fischer, K. Jebens, R. Mugrauer, A. Nagarathinam, F. Scharstein, Artificial hinged-wing bird with active torsion and partially linear kinematics, in: 28th International Congress of the Aeronautical Sciences (ICAS 2012), 2012.
- [3] G.A. Folkertsma, W. Straatman, et al., Robird: a robotic bird of prey, *IEEE Robot. Autom. Mag.* 24 (3) (2017) 22–29.
- [4] J. Gerdes, A. Holness, A. Perez-Rosado, et al., Robo Raven: a flapping-wing air vehicle with highly compliant and independently controlled wings, *Soft Robot.* 1 (4) (2014) 275–288.
- [5] R. Zufferey, J. Tormo-Barbero, M. Guzman, F.J. Maldonado, E. Sanchez-Laulhe, P. Grau, M. Perez, J.Á. Acosta, A. Ollero, Design of the high-payload flapping wing robot E-Flap, *IEEE Robot. Autom. Lett.* 6 (2) (2021) 3097–3104.
- [6] S. Deng, J. Wang, H. Liu, Experimental study of a bio-inspired flapping wing mav by means of force and piv measurements, *Aerosp. Sci. Technol.* 94 (2019) 105382, <https://doi.org/10.1016/j.ast.2019.105382>.
- [7] X. Ke, W. Zhang, J. Shi, W. Chen, The modeling and numerical solution for flapping wing hovering wingbeat dynamics, *Aerosp. Sci. Technol.* 110 (2021) 106474, <https://doi.org/10.1016/j.ast.2020.106474>.
- [8] S. Qin, Z. Weng, Z. Li, Y. Xiang, H. Liu, On the controlled evolution for wingtip vortices of a flapping wing model at bird scale, *Aerosp. Sci. Technol.* 110 (2021) 106460, <http://www.sciencedirect.com/science/article/pii/S1270963820311421>.
- [9] H. Hu, A.G. Kumar, G. Abate, R. Albertani, An experimental investigation on the aerodynamic performances of flexible membrane wings in flapping flight, *Aerosp. Sci. Technol.* 14 (8) (2010) 575–586, <https://doi.org/10.1016/j.ast.2010.05.003>.
- [10] B.-J. Tsai, Y.-C. Fu, Design and aerodynamic analysis of a flapping-wing micro aerial vehicle, *Aerosp. Sci. Technol.* 13 (7) (2009) 383–392, <https://doi.org/10.1016/j.ast.2009.07.007>.
- [11] E. Ajanic, M. Feroshan, S. Mintchev, F. Noca, D. Floreano, Bioinspired wing and tail morphing extends drone flight capabilities, *Sci. Robot.* 5 (47) (2020), <https://doi.org/10.1126/scirobotics.abc2897>.
- [12] S. Ho, H. Nassee, N. Pornsinsirirak, Y.-C. Tai, C.-M. Ho, Unsteady aerodynamics and flow control for flapping wing flyers, *Prog. Aerosp. Sci.* 39 (8) (2003) 635–681.
- [13] Z. Wang, Vortex shedding and frequency selection in flapping flight, *J. Fluid Mech.* 410 (2000) 323–341, <https://doi.org/10.1017/S0022112099008071>.
- [14] H. Wagner, Über die entstehung des dynamischen auftriebes von tragflügeln, *Z. Angew. Math. Mech.* 5 (1) (1925) 17–35, <https://doi.org/10.1002/zamm.19250050103>.
- [15] T. Theodorsen, General theory of aerodynamic instability and the mechanism of flutter, Report, 1934, <https://doi.org/10.1002/zamm.19250050103>.
- [16] I.E. Garrick, On Some Reciprocal Relations in the Theory of Nonstationary Flows, 1938.
- [17] I. Garrick, Propulsion of a flapping and oscillating aerofoil, NACA Report No. 567. Report (United States. National Advisory Committee for Aeronautics), Annual report. 22nd (1936), 1936, pp. 419–427.
- [18] R. Fernandez-Feria, Linearized propulsion theory of flapping airfoils revisited, *Phys. Rev. Fluids* 1 (2016) 084502, <https://doi.org/10.1103/PhysRevFluids.1.084502>.
- [19] R. Jones, The Unsteady Lift of a Wing of Finite Aspect Ratio, 1940.
- [20] J.D. DeLaurier, An aerodynamic model for flapping-wing flight, *Aeronaut. J.* 97 (1964) (1968), <https://doi.org/10.1017/S0001924000026002> (1993) 125–130.
- [21] M.H. Dickinson, K.G. Gotz, Unsteady aerodynamic performance of model wings at low Reynolds numbers, *J. Exp. Biol.* 174 (1) (1993) 45–64.
- [22] S.P. Sane, The aerodynamics of insect flight, *J. Exp. Biol.* 206 (23) (2003) 4191–4208, <https://doi.org/10.1242/jeb.00663>.
- [23] W. Shyy, H. Aono, Recent progress in flapping wing aerodynamics and aeroelasticity, *Prog. Aerosp. Sci.* 46 (7) (2010) 284–327, <https://doi.org/10.1016/j.paerosci.2010.01.001>.
- [24] A. Azuma, The Biokinetics of Flying and Swimming, second edition, American Institute and State University, 2006.
- [25] S. Ansari, R. Źbikowski, K. Knowles, Aerodynamic modelling of insect-like flapping flight for micro air vehicles, *Prog. Aerosp. Sci.* 42 (2) (2006) 129–172, <https://doi.org/10.1016/j.paerosci.2006.07.001>.
- [26] S.A. Ansari, R. Źbikowski, K. Knowles, Non-linear unsteady aerodynamic model for insect-like flapping wings in the hover. Part 1: methodology and analysis, proceedings of the institution of mechanical engineers, Part G, *J. Aerosp. Eng.* 220 (2) (2006) 61–83.
- [27] A. Martin-Alcantara, A simple model for gliding and low-amplitude flapping flight of a bio-inspired uav, in: International Conference on Unmanned Aircraft Systems, ICUAS, 2019, 2006, pp. 729–737.
- [28] D. Chin, D. Lentink, Flapping wing aerodynamics: from insects to vertebrates, *J. Exp. Biol.* 219 (2016) 920–932, <https://doi.org/10.1242/jeb.042317>.
- [29] C. Ellington, C.V.D. Berg, A.P. Willmott, A. Thomas, Leading-edge vortices in insect flight, *Nature* 384 (1996) 626–630.
- [30] H. Liu, C.P. Ellington, K. Kawachi, C. van den Berg, A.P. Willmott, A computational fluid dynamic study of hawkmoth hovering, *J. Exp. Biol.* 201 (4) (1998) 461–477.
- [31] X. Wu, X. Zhang, X. Tian, X. Li, W. Lu, A review on fluid dynamics of flapping foils, *Ocean Eng.* 195 (2020) 106712.
- [32] J. Kou, W. Zhang, Data-driven modeling for unsteady aerodynamics and aeroelasticity, *Prog. Aerosp. Sci.* 125 (2021) 100725.
- [33] S. Brunton, C. Rowley, Empirical state-space representations for theodorsen's lift model, *J. Fluids Struct.* 38 (2013) 174–186.
- [34] M. Zakaria, H. Taha, M.R. Hajj, Measurement and modeling of lift enhancement on plunging airfoils: a frequency response approach, *J. Fluids Struct.* 69 (2017) 187–208, <https://doi.org/10.1016/j.jfluidstructs.2016.12.004>.

- [35] M. Zakaria, H. Taha, M.R. Hajj, A. Hussein, Experimental-based unified unsteady nonlinear aerodynamic modeling for two-dimensional airfoils, <https://doi.org/10.2514/6.2015-3167>, 2015.
- [36] J. Boutet, G. Dimitriadis, Unsteady lifting line theory using the Wagner function for the aerodynamic and aeroelastic modeling of 3d wings, Aerospace 5 (2018) 92, <https://doi.org/10.3390/aerospace5030092>.
- [37] H. Taha, M. Hajj, P. Beran, State-space representation of the unsteady aerodynamics of flapping flight, Aerosp. Sci. Technol. 34 (2014) 1–11.
- [38] H.E. Taha, A.S. Rezaei, On the high-frequency response of unsteady lift and circulation: a dynamical systems perspective, J. Fluids Struct. 93 (2020) 102868.
- [39] W.A. Silva, Discrete-time linear and nonlinear aerodynamic impulse responses for efficient cfd analyses, Dissertation, 1997.
- [40] W.A. Silva, Application of nonlinear systems theory to transonic unsteady aerodynamics responses, J. Aircr. 30 (1993) 660–668.
- [41] A. Jirasek, R. Cummings, Reduced order modeling of x-31 wind tunnel model aerodynamic loads, Aerosp. Sci. Technol. 20 (2010) 52–60, <https://doi.org/10.1016/j.ast.2011.10.014>.
- [42] M. Ghoreyshi, R. Cummings, A. Da Ronch, K.J. Badcock, Transonic aerodynamic load modeling of x-31 aircraft pitching motions, AIAA J. 51 (2013) 2447–2464, <https://doi.org/10.2514/1.J052309>.
- [43] M. Balajewicz, F. Nitzsche, D. Feszty, On the application of multi-input Volterra theory to nonlinear multi-degree-of-freedom aerodynamic systems, AIAA J. 48 (2010) 56–62, <https://doi.org/10.2514/1.38964>.
- [44] K. Liu, D. Li, J. Xiang, Reduced-order modeling of unsteady aerodynamics of a flapping wing based on the Volterra theory, Results Phys. 7 (2017) 2451–2457.
- [45] F. Bos, Numerical simulations of flapping foil and wing aerodynamics: Mesh deformation using radial basis functions, Dissertation, Department of Aerospace Design, Integration and Operations, 2010, ISBN: 9789090251738.
- [46] S. Verma, A. Hemmati, Performance of overset mesh in modeling the wake of sharp-edge bodies, Computation 8 (2020) 66, <https://doi.org/10.3390/computation8030066>.
- [47] A. Gonzalo, G. Arranz, M. Moriche, M. Garcia-Villalba, O. Flores, From flapping to heaving: a numerical study of wings in forward flight, J. Fluids Struct. 83 (2018) 293–309.
- [48] J. Kou, W. Zhang, Comparisons of two reduced-order models for linearized unsteady aerodynamic identification, arXiv:1905.03250, 2019.
- [49] S. Boyd, L. Chua, Fading memory and the problem of approximating nonlinear operators with Volterra series, IEEE Trans. Circuits Syst. 32 (11) (1985) 1150–1161, <https://doi.org/10.1109/TCS.1985.1085649>.
- [50] F.J. Doyle, P.K. Pearson, B.A. Ogunnaike, Identification and Control Using Volterra Models, first edition, Communications and Control Engineering, 2002.
- [51] T. Levi-Civita, Volterra, V. - Theory of functionals and of integral and integrodifferential equations, Scientia 25 (49) (1931) 226.
- [52] S. Van Vaerenbergh, Kernel methods for nonlinear identification, equalization and separation of signals, Ph.D. thesis, 2010.
- [53] S. Orcioni, Improving the approximation ability of Volterra series identified with a cross-correlation method, Nonlinear Dyn. 78 (2014) 2861–2869, <https://doi.org/10.1007/s11071-014-1631-7>.
- [54] T. Treichl, S. Hofmann, D. Schroder, Identification of nonlinear dynamic systems with multiple inputs and single output using discrete-time Volterra type equations, in: Proceedings Fifteenth International Symposium on Mathematical Theory of Networks and Systems, 2002.
- [55] F.J. Maldonado, J.Á. Acosta, J. Tormo-Barbero, M. Guzman, A. Ollero, Adaptive nonlinear control for perching of a bioinspired ornithopter, in: Proceedings of the 2020 IEEE/RSJ International Conference on Intelligent Robots and Systems, IROS, 2020.
- [56] X. Li, Y. Liu, J. Kou, W. Zhang, Reduced-order thrust modeling for an efficiently flapping airfoil using system identification method, J. Fluids Struct. 69 (2017) 137–153.